cmgh
CELLULAR AND MOLECULAR GASTROENTEROLOGY AND HEPATOLOGY

ORIGINAL RESEARCH

NF-κB Inducing Kinase Attenuates Colorectal Cancer by Regulating Noncanonical NF-κB Mediated Colonic Epithelial Cell Regeneration

Holly A. Morrison,[1,*] Kristin Eden,[1,2,*] Brie Trusiano,[1,*] Daniel E. Rothschild,[1] Yufeng Qin,[3] Paul A. Wade,[3] Audrey J. Rowe,[1] Christina Mounzer,[1] Morgan C. Stephens,[1] Katherine M. Hanson,[4] Stephan L. Brown,[4] Eda K. Holl,[5] and Irving C. Allen[1,2,6]

[1]Virginia Tech, Virginia Maryland College of Veterinary Medicine, Department of Biomedical Science and Pathobiology, Blacksburg, Virginia; [2]Virginia Tech, Department of Basic Science Education, Virginia Tech Carilion School of Medicine, Roanoke, Virginia; [3]National Institute of Environmental Health Sciences, Research Triangle Park, North Carolina; [4]Via College of Osteopathic Medicine, Department of Cell Biology and Physiology, Spartanburg, South Carolina; [5]Duke University, Department of Surgery, Durham, North Carolina; and [6]Graduate Program in Translational Biology, Medicine and Health, Virginia Polytechnic Institute and State University, Roanoke, Virginia

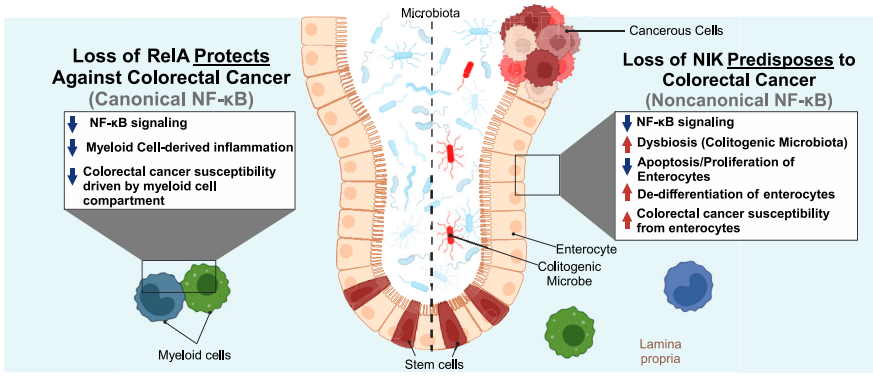

SUMMARY

NF-κB-inducing kinase (NIK) is a critical regulator of colonic epithelial cell (CEC) regeneration, and loss of NIK predisposes cells to malignant transformation. During colorectal cancer, NIK attenuation results in altered maturation of colonic stem cells (CSCs), which are likely more susceptible to mutation and malignant transformation, giving rise to neoplastic CECs.

BACKGROUND & AIMS: Dysregulated colonic epithelial cell (CEC) proliferation is a critical feature in the development of colorectal cancer. We show that NF-κB-inducing kinase (NIK) attenuates colorectal cancer through coordinating CEC regeneration/differentiation via noncanonical NF-κB signaling that is unique from canonical NF-kB signaling.

METHODS: Initial studies evaluated crypt morphology/functionality, organoid generation, transcriptome profiles, and the microbiome. Inflammation and inflammation-induced tumorigenesis were initiated in whole-body NIK knockout mice ($Nik^{-/-}$) and conditional-knockout mice following administration of azoxymethane and dextran sulfate sodium.

RESULTS: Human transcriptomic data revealed dysregulated noncanonical NF-kB signaling. In vitro studies evaluating $Nik^{-/-}$ crypts and organoids derived from mature, nondividing CECs, and colonic stem cells exhibited increased accumulation and stunted growth, respectively. Transcriptomic analysis of $Nik^{-/-}$ cells revealed gene expression signatures associated with altered differentiation-regeneration. When assessed in vivo, $Nik^{-/-}$ mice exhibited more severe colitis with dextran sulfate sodium administration and an altered microbiome characterized by increased colitogenic microbiota. In the inflammation-induced tumorigenesis model, we observed both increased tumor burdens and inflammation in mice where NIK is knocked out in CECs ($Nik^{\Delta CEC}$). Interestingly, this was not recapitulated when NIK was conditionally knocked out in myeloid cells ($Nik^{\Delta MYE}$). Surprisingly, conditional knockout of the canonical pathway in myeloid cells ($RelA^{\Delta MYE}$) revealed decreased tumor burden and inflammation and no significant changes when conditionally knocked out in CECs ($RelA^{\Delta CEC}$).

CONCLUSIONS: Dysregulated noncanonical NF-κB signaling is associated with the development of colorectal cancer in a tissue-dependent manner and defines a critical role for NIK in regulating gastrointestinal inflammation and regeneration associated with colorectal cancer. *(Cell Mol Gastroenterol Hepatol 2024;18:101356; https://doi.org/10.1016/j.jcmgh.2024.05.004)*

Keywords: Colitis-Associated Tumorigenesis; Differentiation; Organoids; Epithelial Cells.

The transcription factor nuclear factor kappa B (NF-κB) is an essential regulator of biological processes in the gastrointestinal (GI) system. The NF-κB signaling pathways have been well-studied in a variety of GI diseases.[1–11] NF-κB signaling proceeds through 2 distinct pathways, the canonical and noncanonical pathways.[12–14] To date, the majority of studies have focused on canonical NF-κB signaling in the gut. In canonical NF-κB signaling, (RelA/p65)/p50 heterodimers are maintained in an inactive state in the cytoplasm by a family of inhibitors of NF-κB (IκBα). On activation, the large IκB kinase complex consisting of the IκB kinase γ (NEMO), IκB kinase α (IKKα), and IκB kinase β (IKKβ) phosphorylates IκBα, resulting in its degradation and release of the RelA/p50 heterodimer. This heterodimer rapidly translocates into the nucleus, driving the transcription of a large repertoire of mediators that control diverse biological processes, including inflammation, cell death, and proliferation.

Unlike canonical NF-κB, there is a relative lack of data associated with noncanonical NF-κB signaling, because noncanonical NF-κB was originally considered an auxiliary signaling mechanism to canonical NF-κB. Noncanonical NF-κB signaling is associated with the p52/RelB heterodimer. p52 is maintained in a precursor form as p100 and acts as an IκB-like molecule that restricts RelB to the cytoplasm. On receptor stimulation, p100 is degraded by the proteasome and processed to p52, which unmasks the nuclear localization sequence and facilitates nuclear translocation. Processing of p100 to p52 is tightly regulated by the essential NF-κB–inducing kinase (NIK). Under normal conditions, NIK is constitutively degraded via a multiprotein regulator complex consisting of tumor necrosis factor (TNF)-receptor associated factor 3 (TRAF3), TRAF2, and cellular inhibitor of apoptosis 1 and 2, which prevents basal activation of noncanonical NF-κB signaling. On recognition of an upstream TNF family signaling molecule, TRAF3 is degraded, and NIK becomes stabilized, allowing it to phosphorylate IKKα. IKKα subsequently phosphorylates p100, resulting in ubiquitination and proteasome cleavage into active p52. The p52/RelB heterodimer initiates the transcription of a relatively limited set of target genes that are distinct from those targeted by the canonical NF-κB subunits. Several chemokines are well-defined targets of noncanonical NF-κB signaling, including CXCL12, CXCL13, CCL19, and CCL21.[5,15] In regard to studies involving the GI tract, most studies have focused on both conventional and cell-type specific NIK knockout mice, because these murine models have significant phenotypes in the GI system. For example, the most defined biological function attributed to noncanonical NF-κB signaling is the development and organization of secondary lymphoid structures such as Peyer's patches.[16–20] In mice with a mutation in NIK that blocks noncanonical NF-κB signaling or lacking lymphotoxin β receptor upstream of NIK, lymph nodes and Peyer's patches are significantly underdeveloped or lacking entirely.[20] In addition, disruption of NIK has also been linked to a systemic inflammatory condition in mice, characterized as a hypereosinophilic syndrome–like disease with progressive eosinophilia, tissue destruction, and premature death.[4] Consequently, during the early stages of this disorder, mice develop upper GI phenotypes that effectively model key aspects of eosinophilic esophagitis, including clinically relevant esophageal-specific eosinophil recruitment and remodeling.[3]

In the context of the lower GI tract, when NIK is conditionally deleted in colonic epithelial cells (CECs) using Cre recombinase under the control of the *Villin* promoter, these mice were found to be more susceptible to local and systemic inflammation in inflammatory bowel disease (IBD) and sepsis models.[21] The mechanism associated with this susceptibility was found to be associated with improper maintenance and differentiation of microfold cells (M-cells) in the epithelial cell barrier. Loss of epithelial cell NIK resulted in decreases in interleukin (IL) 17 expression and immunoglobulin A coating of colitogenic bacteria, resulting in increased GI inflammation.[21] This is also worth noting because noncanonical NF-κB signaling can also modulate T-cell differentiation, B-cell development and function, immunoglobulin A class switching, dendritic cell development, cell migration, chemokine production, and interferon signaling.[21–28] Although the findings in conditional knockout models characterized a role for NIK in CECs and gut health homeostasis, these changes were only assessed during the acute phase of dextran sulfate sodium (DSS) induced inflammation. Its role during chronic inflammation and in the context of relapsing, remitting disease was not assessed. Furthermore, noncanonical versus canonical signaling was not compared between CECs and the myeloid compartment, aside from bone marrow chimera studies assessing systemic *Nik*$^{-/-}$ mice.[21]

Expanding the role of NIK and noncanonical NF-κB signaling beyond inflammatory diseases, this pathway has also been evaluated in the context of cancer in a few limited studies, including assessments of CD8+ effector T-cell

*Authors share co-first authorship.

Abbreviations used in this paper: **AOM/DSS, azoxymethane and dextran sulfate sodium; CEC, colonic epithelial cell; CRC, colorectal cancer; CSC, colonic stem cell; GI, gastrointestinal; HT, healthy tissue; IBD, inflammatory bowel disease; IκB, inhibitor of kappa B; IL, interleukin; IPA, Ingenuity Pathway Analysis; LDA, linear discriminant analysis; LT, lesion tissue; NIK, NF-κB-inducing kinase; NF-κB, nuclear factor B; TCGA, The Cancer Genome Atlas; TNF, tumor necrosis factor; TRAF, TNF-receptor associated factor.**

Most current article

2352-345X
https://doi.org/10.1016/j.jcmgh.2024.05.004

function in the tumor microenvironment.[29] However, the role of NIK and noncanonical NF-κB signaling has not been characterized in the context of GI neoplasia. Here, we show that NIK attenuates colorectal cancer (CRC) through the regulation of noncanonical NF-κB mediated maintenance of CEC regeneration, differentiation, and maturation. In novel genetically modified mice, we illustrate that noncanonical NF-κB signaling is essential for protection against CRC and functions through the epithelial cell compartment. Conversely, canonical NF-κB signaling in the myeloid cell compartment augments CRC progression via enhanced tumor promoting inflammation. In the absence of NIK, improper CEC differentiation, regeneration, and maturation allow damage to accumulate, promoting enhanced dysplasia that contributes to malignant transformation.

Results

Noncanonical NF-κB Signaling Is Attenuated in Human Colorectal Cancer Patients

Noncanonical NF-κB signaling is differentially regulated in human patients with a variety of GI disorders.[2,3] Therefore, we first sought to evaluate noncanonical NF-κB signaling in human CRC patients. Using Oncomine, GEO data sets, CompBio, and Ingenuity Pathway Analysis (IPA), we conducted a series of retrospective metadata analyses of gene expression profiles in CRC patients (Figure 1). Here, in an unbiased approach, we evaluated 80 known components or modifiers of the noncanonical NF-κB signaling pathway at multiple levels, including ligand-receptor interactions, pathway components, regulators, and effectors. The most

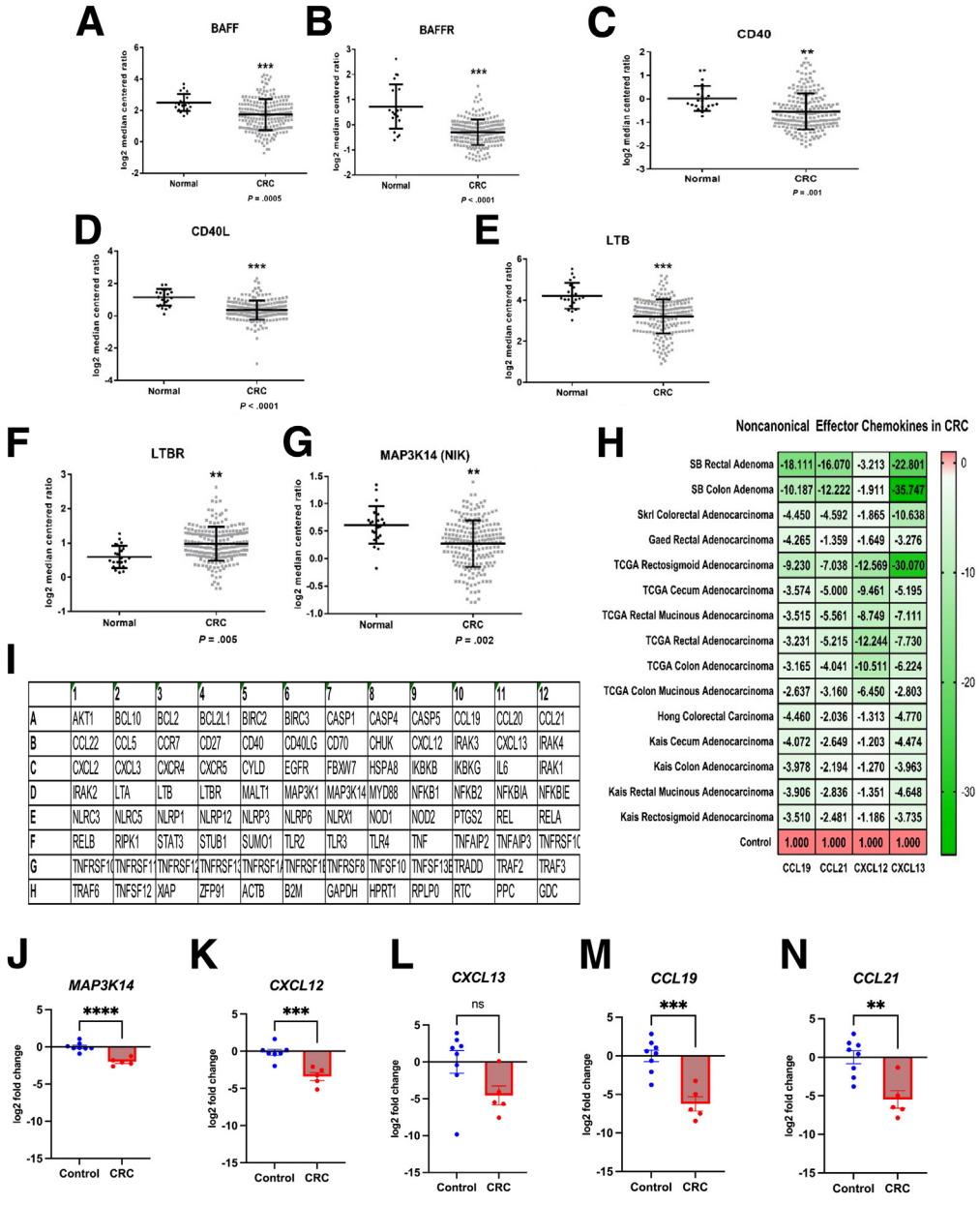

Figure 1. Noncanonical NF-κB signaling is attenuated in human colorectal cancer patients. (*A–H*) Data from the TCGA data sets were analyzed, and the expression of key genes associated with noncanonical NF-κB signaling was compared between normal healthy controls (n = 22) and CRC patients (n = 215). Significant changes were observed in (*A*) *BAFF*, (*B*) *BAFFR*, (*C*) *CD40*, (*D*) *CD40L*, (*E*) *LTB*, (*F*) *LTBR*, and (*G*) *MAP3K14* (NIK). (*H*) Using TCGA data sets, the gene expression levels of 4 effector chemokines produced by noncanonical NF-κB signaling (CCL19, CCL21, CXCL12, and CXCL13) were analyzed across different types of CRC. Data sets were only included if they contained all 4 chemokines. Significance was defined as ±2-fold change in expression. (*I*) RNA from human colon biopsies (n = 6 control, 6 CRC) were pooled and analyzed using a custom Superarray containing the 80 genes evaluated in the metadata analysis. (*J–N*) Data from the retrospective studies were confirmed by reverse transcriptase-polymerase chain reaction from colon biopsies from CRC patients (n = 6 control, 6 CRC). $^{**}P < .01$; $^{***}P < 0.005$; $^{****}P < .001$.

comprehensive data analysis used the largest data set available across platforms, The Cancer Genome Atlas (TCGA), which is composed of 215 CRC biopsy samples and 22 control tissues (Figure 1). All 80 genes evaluated were significantly dysregulated in the CRC patients, with 11 genes (13.75%) identified as being significantly dysregulated across all platforms and analyses (Figure 1). B-cell activating factor (*BAFF*) (Figure 1*A*), its receptor *BAFFR* (Figure 1*B*), the noncanonical receptor cluster of differentiation 40 (*CD40*) (Figure 1*C*), its ligand *CD40L* (Figure 1*D*), and lymphotoxin beta (*LTB*) (Figure 1*E*), which are all potent stimulators of noncanonical NF-κB signaling, were all significantly down-regulated in biopsy samples from CRC patients. However, the gene encoding the LTB receptor, *LTBR*, was the sole gene consistently found significantly up-regulated in CRC patients (Figure 1*F*). In the signaling pathway, NIK, encoded by the gene *MAP3K14*, is also significantly down-regulated in CRC patients (Figure 1*G*). We next investigated the expression of downstream chemokines of noncanonical signaling not only within the TCGA data set but across multiple CRC data sets available on Oncomine where these 4 genes were expressed and included in the data sets. Here, we observed the 4 most common chemokines associated with noncanonical NF-κB signaling, *CXCL12, CXCL13, CCL19*, and *CCL21*, consistently and significantly down-regulated across data sets, including different subsets of CRC (Figure 1*H*).

Validating the metadata analysis, we acquired RNA extracted from formalin-fixed paraffin-embedded tissue of colonic biopsies from 6 human CRC patients and 6 control (non-inflamed, non-neoplastic) biopsies. RNA was pooled and then analyzed using a custom Superarray containing the 80 genes evaluated in the metadata analysis (Figure 1*I*). Consistent with the metadata analysis, significant differences between CRC patients and controls were observed for all 80 genes, with the majority being down-regulated. Specifically, *NIK* and the 4 noncanonical chemokines were all significantly down-regulated in our CRC patients compared with the control specimens (*NIK*, −2.59 fold; *CXCL12*, −3.67 fold; *CXCL13*, −7.34 fold; *CCL19*, −59.28 fold; and *CCL21*, −30.02 fold) (Figure 1*J*–*N*).

To further explore these findings, we used IPA and confirmed that noncanonical signaling was significantly suppressed in the CRC patients at multiple points, specifically *MAPK314*, *RELB*, and all 4 chemokines (Figure 2*A* and *B*). Conversely, there appeared to be some potential compensatory up-regulation in *CXCR4* and *CXCR5*, which are the receptors for CXCL12 and CXCL13 (Figure 2*B*). In addition, A20 (*TNFAIP3*) and several additional members of the NOD-like receptor signaling family were also identified as critical signaling hubs/regulators of both canonical and noncanonical signaling and were subsequently significantly dysregulated in our CRC patients (Figure 2*C*). Also of note is the up-regulation of *NLRP12*, which functions as a suppressor of noncanonical NF-κB signaling (Figure 2*D*). On the basis of the global changes in gene expression, IPA also predicted 3 pharmacologic agents, romidepsin, S-nitrosoglutathione, and methotrexate, that may impact key aspects of noncanonical NF-κB signaling that were significantly altered in our CRC patient populations (Figure 2*E*). These findings were previously confirmed using individual real-time polymerase chain reaction for *NIK (MAP3K14)*, *CXCL12, CXCL13, CCL19*, and *CCL21* (Figure 1*J*–*N*). A schematic of these results is further summarized in Figure 2*F*. Overall, these results demonstrate that dysregulated noncanonical and canonical NF-kB signaling is found in CRC patients. Specifically, we see down-regulation of key components of noncanonical signaling including TNFR ligands, *NIK*, and resultant cytokines with concurrent up-regulation of NLRP12. This suggests that loss of noncanonical NF-κB signaling and concurrent dysregulated canonical NF-κB signaling may be associated with the development of CRC.

NIK and Noncanonical NF-κB Signaling Regulates Colonic Epithelial Cell Regeneration and Turnover

Next, we assessed the physiological implications of the observations detailed above and functionally defined the impact of defective noncanonical NF-κB signaling and loss of NIK in CECs. Here, we isolated and evaluated whole crypts from whole-body $Nik^{-/-}$ and wild-type mice to evaluate the role of NIK in maintaining crypt development, including the balance of colonic stem cell (CSC) proliferation and CEC differentiation. Immunohistochemistry for Ki-67 revealed intense staining near the bottom of the crypts from wild-type mice (Figure 3*A*), consistent with the normally high levels of proliferation and regeneration in the crypt niche. However, Ki-67 staining was significantly decreased in the crypts isolated from the $Nik^{-/-}$ animals (Figure 3*A*). Indeed, quantification of Ki-67 immunohistochemistry revealed a 4.375-fold decrease in Ki-67 staining in the $Nik^{-/-}$ crypts compared with those from wild-type mice (Figure 3*B*). We also observed a significant decrease in *Lgr5* expression, which is a CSC marker, in the $Nik^{-/-}$ crypts compared with wild-type crypts (Figure 3*C*). Together, these data suggest reduced proliferation in the $Nik^{-/-}$ crypts compared with wild-type counterparts in vitro. Subsequent morphologic analysis also consistently revealed significant elongation of the $Nik^{-/-}$ crypts compared with wild-type crypts (Figure 3*A* and *D*). $Nik^{-/-}$ crypts averaged almost twice the length of the wild-type crypts (Figure 3*D*). We next evaluated the expression of cytokeratin 20 (*Krt20*), which is a marker of mature enterocytes, and found significantly increased levels in $Nik^{-/-}$ crypts (Figure 3*E*). The colonic crypts of $Nik^{-/-}$ mice also had decreased expression of poly-ADP ribose (PARP1) and its cleaved product (cPARP1) (Figure 3*F*). These findings suggest that elongation of crypts is associated with accumulation of cells with a mature, non-dividing phenotype that are more resistant to apoptosis in $Nik^{-/-}$ mice.

To better characterize these differences, we next generated colon organoids from stem cells isolated from wild-type, $Nik^{-/-}$, and Apc^{min} animals. Culturing colonic organoids generates an epithelial-cell only population that arises from isolated stem cells and differentiates into all the various epithelial-cell types of the colonic mucosa including enterocytes, goblet cells, and Paneth cells. The Apc^{min} mice

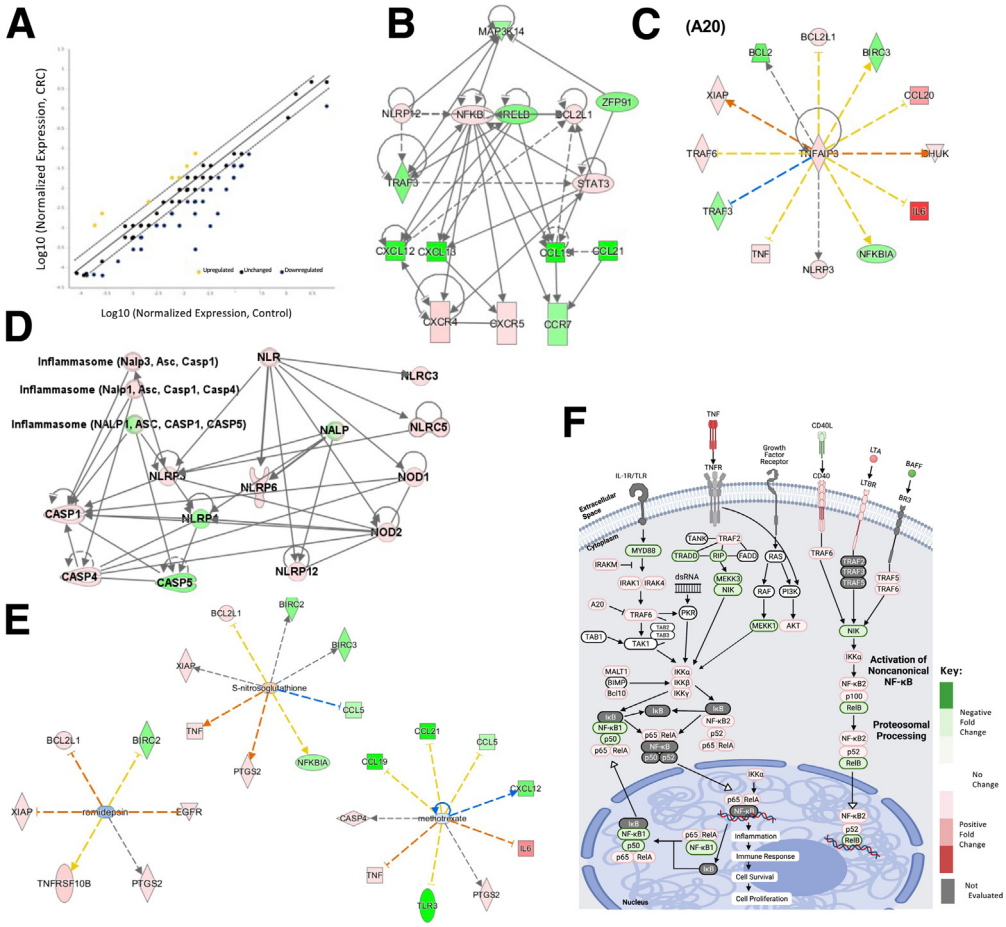

Figure 2. Noncanonical NF-κB signaling is significantly down-regulated in biopsies from CRC patients. (*A*) RNA was extracted from human colon biopsies (n = 6 control; n = 6 CRC), and gene expression was evaluated using custom NF-κB signaling Superarray. Compared with control tissue, tissue from CRC patients showed a general down-regulation of genes related to noncanonical signaling (*A*; *yellow*, up-regulation; *blue*, down-regulation). *Solid line* represents no change from control, and *each dotted line* marks the borders of likely physiological significance (ie, change in fold regulation of >2). (*B–E*) Gene expression data from the GEO data set was evaluated using IPA. (*B*) IPA confirmed that noncanonical NF-κB signaling was significantly down-regulated and identified NIK (*MAP3K14)* as a critical driver of this dysregulation. (*C*) A20 and (*D*) NOD-like receptor signaling were identified as significant regulatory hubs for the altered NF-κB signaling identified by IPA. (*B–D*) *Red* correlates to up-regulation, and *green* correlates to down-regulation. (*C–E*) *Solid lines* indicate a direct interaction, *dotted lines* indicate an indirect interaction, *arrowheads* on the end of the line indicate activation, and *flat lines* on the end indicate inhibition. For colors, *orange lines* indicate a straightforward predicted activation, and *blue lines* indicate a straightforward predicted inhibition. *Yellow lines* indicate a more complex relationship with some inconsistencies in relationships that might indicate additional players. *Grey lines* indicate an effect is not predicted. (*E*) Based on the gene expression changes identified by IPA, romidepsin, s-nitrosoglutathione, and methotrexate were predicted by IPA to potentially impact disease progression. (*F*) Schematic of key aspects of noncanonical NF-κB signaling that were significantly altered in our CRC patient population. n = 6 control; n = 6 CRC human patients used in Superarray. Significant values ≥2 (*yellow/red*) and ≤2 (*blue/green*) reported as fold-change.

lack a negative regulator of the canonical Wnt/β-catenin signaling pathway, resulting in the up-regulation of the WNT pathway. This mechanism is strongly associated with stem cell proliferation and self-renewal at the base of the intestinal crypts.[30] Thus, they are used here as positive controls for stem-cell hyperproliferation in the organoids. Colonic crypt stem cells from each mouse line were collected and cultured for 6 days, with size measurements conducted over time. Wild-type organoids formed at a highly consistent rate and grew to a predictable size over the 6-day period (Figure 3*G*). Organoids from the Apc^{min} mice demonstrated significantly accelerated epithelial cell proliferation between days 3 and 4 (Figure 3*G*), consistent with the Wnt signaling dysregulation and subsequent stem cell hyperproliferation. The Apc^{min} organoids maintained a diameter that was approximately double that of the wild-type organoids throughout the remainder of the study (Figure 3*G*). Conversely, organoids from the $Nik^{-/-}$ mice demonstrated significantly attenuated proliferation and growth beyond day 4 (Figure 3*G*). Diameter measurements revealed that

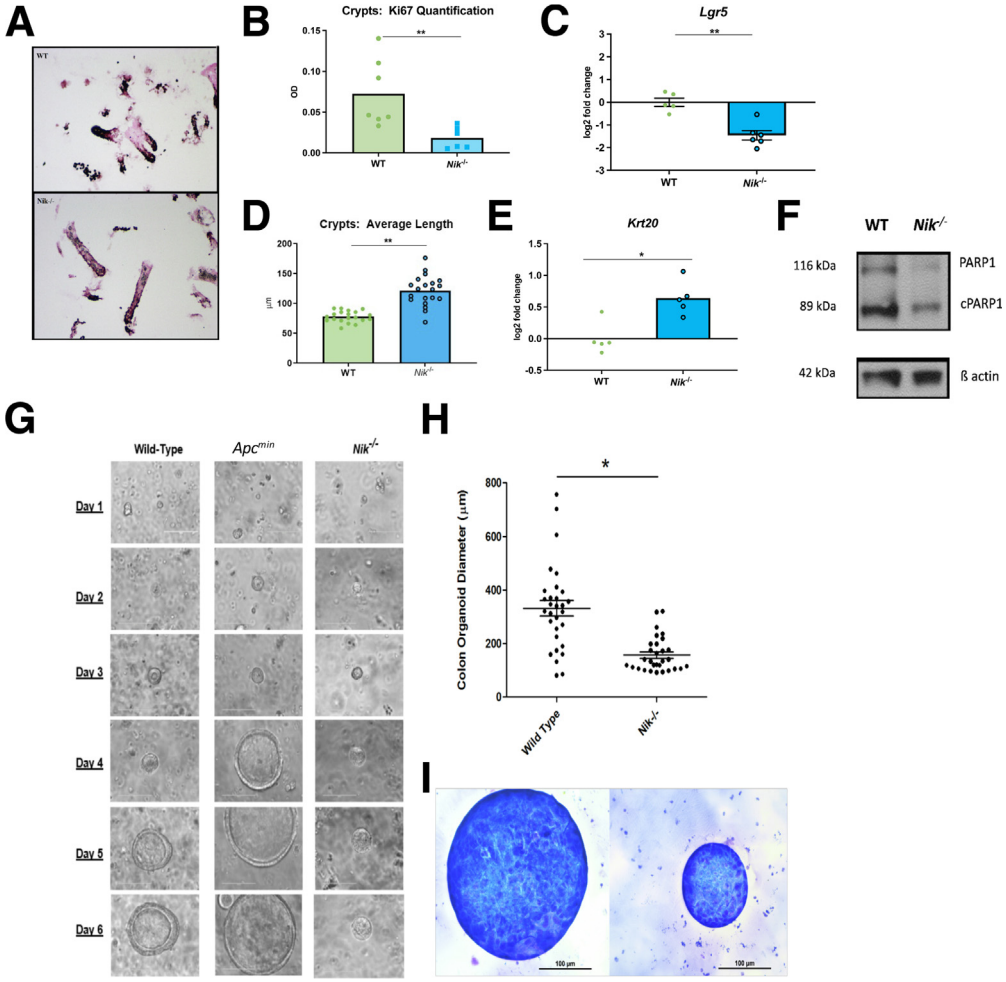

Figure 3. Colonic crypts from *Nik*$^{-/-}$ mice display decreased levels of stem cell proliferation and mature colonic epithelial cell death. (*A* and *B*) Immunocytochemistry of wild-type and *Nik*$^{-/-}$ crypts revealed decreased Ki-67 expression in the crypt base. (*C*) *Lgr5* gene expression was significantly attenuated in the *Nik*$^{-/-}$ crypts. (*D*) Crypts from the *Nik*$^{-/-}$ animals were significantly elongated compared with those from wild-type mice. (*E*) Krt20 gene expression was significantly increased in the *Nik*$^{-/-}$ crypts. (*F*) Western blot analysis of the crypt fractions revealed decreased mature and cleaved poly-ADP ribose (PARP) levels in the *Nik*$^{-/-}$ crypts compared with wild-type. (*G*) Organoids from *Apc*^{min} mice displayed typical overzealous proliferation, whereas wild-type organoid growth was steady and highly uniform. *Nik*$^{-/-}$ organoids remained small compared with both wild-type and *Apc*^{min}. Colonic crypts were isolated and reduced to a single-cell suspension from wild-type, *Nik*$^{-/-}$, and *Apc*^{min} mice and grown in culture for 6 days, without passage. (*H*) Blinded diameter measurement of randomly chosen organoids from wild-type and *Nik*$^{-/-}$ mice. (*I*) Organoids were manually disassociated from Matrigel and stained cytologically with Diff-Quik to evaluate morphology (wild-type/*left*; *Nik*$^{-/-}$/*right*) despite the difference in size. Data represent the average of 3 independent trials. Measurements were taken from 30 randomly chosen organoids spread over a total of 12 wells. *$P \leq .05$.

the *Nik*$^{-/-}$ organoids were significantly smaller, averaging approximately half of the size of the wild-type organoids (Figure 3*H*). Despite the smaller size, the *Nik*$^{-/-}$ organoids were still composed of live cells and demonstrated similar morphology when compared with the wild-type and *Apc*^{min} organoids (Figure 3*I*). *Nik*$^{-/-}$ organoids were also similar in number to the wild-type and Apc^{min} organoids, only smaller in size (Figure 3*I*, data not shown). Together, these data suggest that *Nik*$^{-/-}$ in CSCs may be associated with a deficiency in progenitor activity and concurrent maturation aberrancies that result in a mature phenotype earlier on in CEC development. Therefore, we postulated that this could result in enhanced tumorigenesis under inflammatory conditions.

NIK Functions to Attenuate Experimental Colitis and Colon Inflammation

Because of its effects in human patients and on crypts and organoids in vitro, we next assessed the in vivo role of NIK in maintaining GI homeostasis in the colon. Because of the prior phenotypes described for the *Nik*$^{-/-}$ mice,[29,31,32] we assessed the colons histologically and noted that the resting colon in vivo was phenotypically similar between the *Nik*$^{-/-}$ and wild-type animals between 8–12 weeks of age (Figure 4*A* and *B*). Histologically, colons collected from wild-type mice and *Nik*$^{-/-}$ mice were also similar in vivo despite the morphologic differences we noted in vitro (Figure 4*A* and *B*). For both groups of mice before colitis induction in vivo, there appeared to be normal distributions of

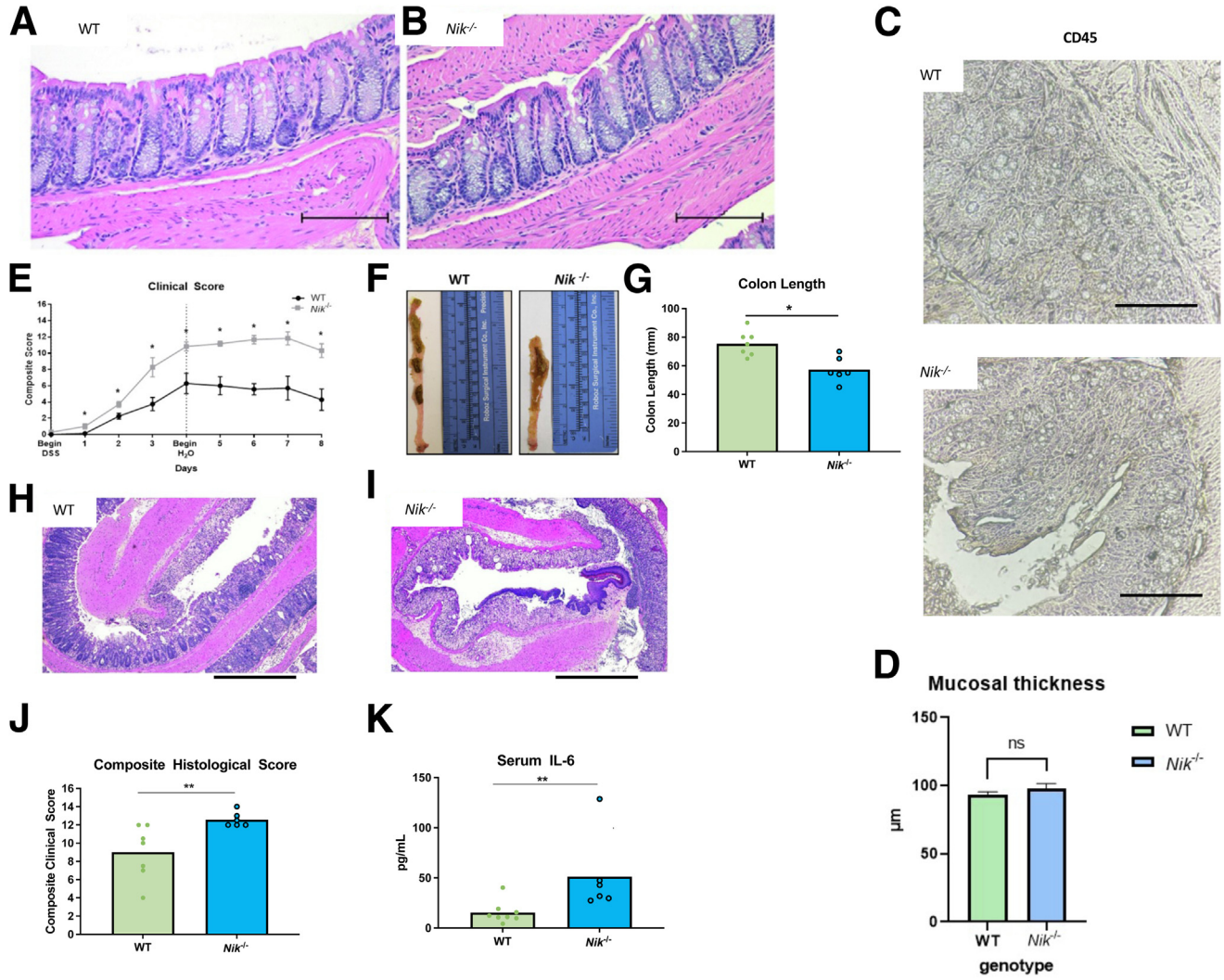

Figure 4. *Nik*$^{-/-}$ mice are sensitive to DSS-induced experimental colitis. (*A*) Wild-type (WT) mice and (*B*) *Nik*$^{-/-}$ mice display almost identical architecture, with healthy crypts and lack of inflammation under unstimulated conditions at the time points evaluated in the AOM+DSS study. Scale bars represent 100 μm. (*C*) Wild-type and *Nik*$^{-/-}$ mice exhibit minimal leukocyte infiltration into the crypts and villi at baseline demonstrated by CD45 staining. Original magnification, ×40; scale bars represent 100 μm. (*D*) *Nik*$^{-/-}$ mice and WT mice exhibit no significant differences between mucosal thickness, confirming no significant morphologic or pathologic differences at baseline. N = 8–9 mice/group. Each histologic sample from each mouse had the mucosal depth measured from the crypt up to the villus tip at 5 randomly chosen histologic areas. (*E*) *Nik*$^{-/-}$ mice exposed to 5% DSS in the acute experimental colitis model demonstrated enhanced clinical features of disease progression (weight loss, blood in stool, stool consistency, body condition, and behavior) compared with wild-type mice. (*F* and *G*) Colon length, a typical gross marker of inflammation and damage, was significantly decreased in the *Nik*$^{-/-}$ mice. (*H* and *I*) Histopathology assessments revealed increased inflammation in the *Nik*$^{-/-}$ colons, including increased damage to the epithelial cell barrier, compared with wild-type. (*J*) Semiquantitative scoring of pathology, assessing inflammation, epithelial cell defects, dysplasia, hyperplasia, which was translated into a composite score as previously described.[33] (*K*) Serum cytokine levels were evaluated by enzyme-linked immunosorbent assay, with significant increases in IL-6 observed in the *Nik*$^{-/-}$ mice compared with the wild-type animals. n = 6; wild-type, n = 7. **P* ≤ .05; ***P* ≤ .01.

enterocytes, no evident inflammatory reaction, and comparable mucosal thicknesses (Figure 4*C* and *D*).

A previous study has shown that negative regulators of NIK can suppress colon inflammation through attenuating noncanonical NF-κB signaling.[5] Conversely, NIK has been shown to attenuate experimental colitis and sepsis progression through the CEC compartment.[21] Thus, we sought to directly evaluate these findings using the *Nik*$^{-/-}$ mice in a model of DSS-induced experimental colitis.[34] Male *Nik*$^{-/-}$ and littermate *Nik*$^{+/+}$ mice were used in all studies. Mice were administered 5% DSS for 4 days and allowed to recover for 4 additional days to allow epithelial cell regeneration (Figure 4*E*–*K*). Clinical scores, which are composite scores of activity levels, fecal consistency, blood in stool, and weight loss, were generated daily for each mouse in the study.[5] *Nik*$^{-/-}$ mice had significantly increased clinical scores at all

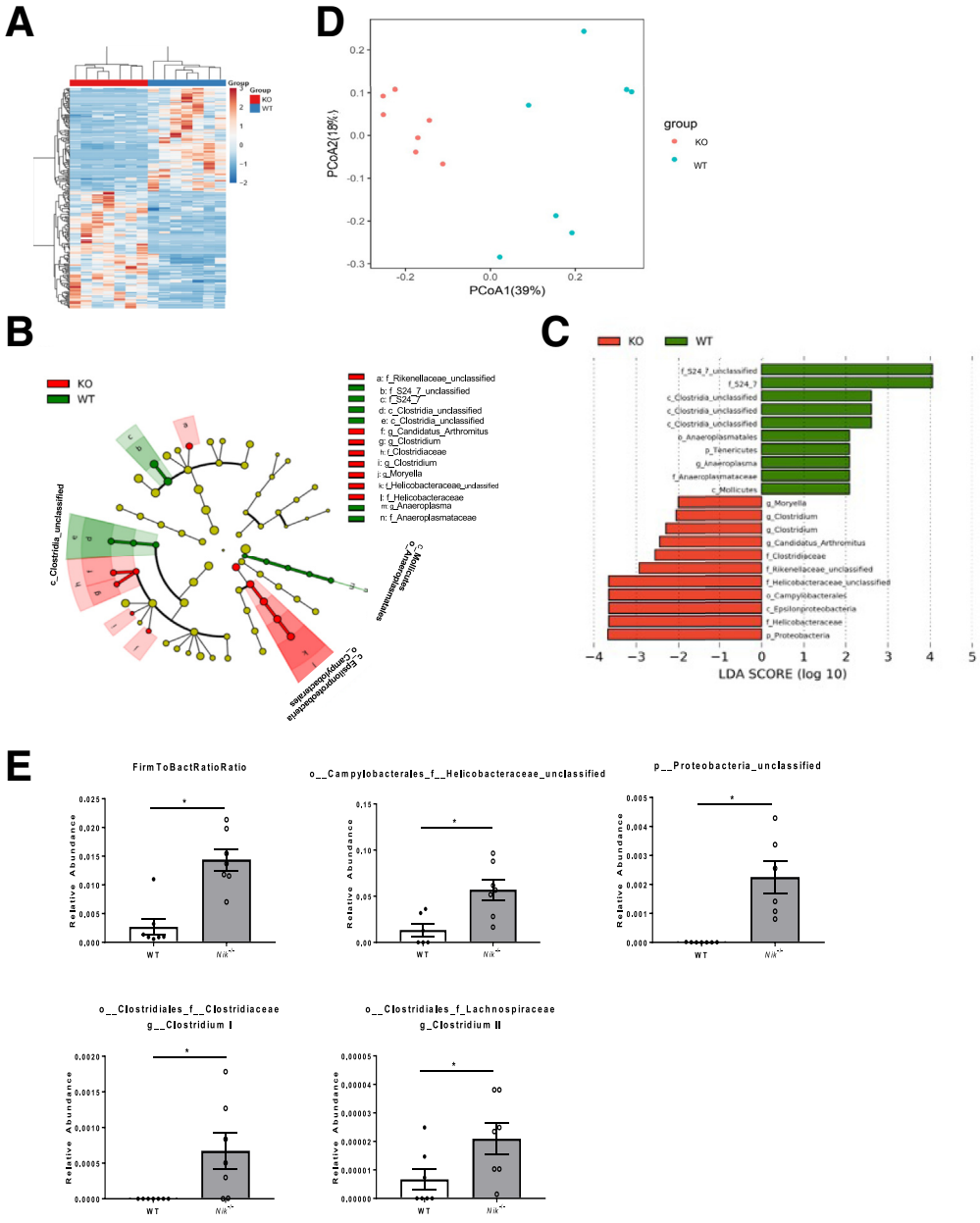

Figure 5. *Nik*$^{-/-}$ mice display an altered microbiome with differential expression of species important to gut health. (*A*) The operational taxonomic unit heatmap shows hierarchical clustering associated with altered expression patterns of different bacterial taxa in the colonic contents of *Nik*$^{-/-}$ mice versus wild-type littermates. *Red* represents KO samples, and *blue* represents WT samples (KO = *Nik*$^{-/-}$, WT = wild-type). (*B*) The phylogenic tree reveals the relationships between different orders, families, and genera that were changed in the *Nik*$^{-/-}$ and wild-type microbiomes. (*C*) The LDA score is a measure of bacterial species abundance. An LDA score of more than 2-fold change is considered significant. *Nik*$^{-/-}$ and wild-type mice exhibited different patterns of bacteria abundance, with particular emphasis on Clostridia, *Helicobacter*, and Camplylobacter. (*D*) PCA graph shows distinct clustering based on genotype. (*E*) Increased Firmicutes to Bacteroidetes ratio and unclassified bacteria in *Nik*$^{-/-}$ mice. n = 7 mice per genotype. Significance was defined as $P \leq .05$.

monitoring points, indicating that NIK plays a critical function in attenuating experimental colitis progression (Figure 4*E*). The colons of *Nik*$^{-/-}$ mice were significantly shortened and contained poorly formed fecal material (Figure 4*F* and *G*). Histologically, wild-type mice showed significant ulceration and inflammation and the beginnings of crypt reformation (Figure 4*H*). However, we observed significantly increased colon inflammation and CEC ulceration in the *Nik*$^{-/-}$ mice, which were histopathologically assessed and quantified using a composite score, as previously described[33] (Figure 4*I* and *J*). In addition, the systemic effects of this ulceration and inflammation were more significant in the *Nik*$^{-/-}$ mice, as evidenced by increased serum levels of IL-6 (Figure 4*K*).

To then evaluate whether underlying dysbiosis drives increased inflammation and epithelial cell barrier damage, fecal pellets were collected from *Nik*$^{-/-}$ and wild-type littermates before induction of colitis. The mice displayed distinct patterns of bacterial taxa (Figure 5*A* and *D*) that are commonly associated with dysbiosis. Using linear discriminant analysis (LDA), we found significant differences (ie, greater than 2 LDA score) in several bacteria species (Figure 5*B* and *C*). Clostridial species appeared to be a major family of interest. Whereas unclassified members of the class Clostridium were identified as being overexpressed in wild-type mice, there were 2 specific genera of Clostridium and 1 unclassified Clostridiaceae family member that were overabundant in the *Nik*$^{-/-}$ mice (Figure 5*B*, *C*, and *E*). Clostridial bacteria are important in colonic homeostasis and can have both protective and proinflammatory effects, depending on species and the overall proportion of those species within

the gut.[35] Another important bacterial family that was overexpressed in the *Nik*$^{-/-}$ colon is Helicobacterceae (Figure 5*B*, *C*, and *E*). *Helicobacter* has been implicated in many GI diseases, including cancer formation.[36] Other elevated microbiota in the *Nik*$^{-/-}$ mice included bacteria of the order Campylobacterales and bacteria within the phylum Proteobacteria, the latter of which has been associated with Crohn's disease and compromised mucous barriers in mouse colons (Figure 5*C* and *E*).[37] Additional bacteria also included *Moryella*, *Candidatus arthromitus*, *Rikinella*, and Epsilonproteobacteria (Figure 5*B* and *C*). In addition to these findings, *Nik*$^{-/-}$ mice had a significantly increased Firmicutes to Bacteroidetes ratio, which is also noted in cases of dysbiosis (Figure 5*E*).[35] Together, these data suggest that the baseline microbiome is altered and favors dysbiosis in the GI tract of the *Nik*$^{-/-}$ mice. However, this skewing does not appear to cause significant inflammatory or structural changes to the GI mucosa in health but may partially exacerbate the robust inflammation observed in the experimental colitis model. On the basis of the skewed microbiome, we predict that these mice may also have altered immunologic and epithelial phenotypes within the GI tract as well.

NIK Attenuates Colitis-associated Colorectal Cancer Through Colonic Epithelial Cells

As we demonstrated above, mice lacking NIK and noncanonical NF-κB signaling are more sensitive to DSS-induced experimental colitis. These data are consistent with prior studies using conditional-knockout mice, where epithelial NIK was shown to protect against colon inflammation and sepsis through the maintenance of M cells.[21] Specifically, these prior studies used conditional-knockout mice where *Nik* deletion was driven by Cre under the control of the epithelial *Villin* promoter. On the basis of these data and our findings in human cancer patients, we next defined the role of NIK in CRC using cell-type specific conditional-knockout animals in evaluating tumorigenesis via the azoxymethane (AOM)+DSS model. We generated a novel mouse line carrying a *Nik* locus that is sensitive to disruption by Cre recombinase (Figure 6*A*). Briefly, key regions of the *Map3k14* (*Nik*) gene were flanked by loxP sites (*Nik*$^{fl/fl}$), resulting in the deletion of exons 7 and 8 in cells where Cre recombinase is expressed (Figure 6*A*). On the basis of the findings from our studies using whole-body *Nik*$^{-/-}$ mice and prior in vitro studies focused on epithelial cells, we generated mice lacking *Nik* in the CEC compartment by crossing our *Nik*$^{fl/fl}$ mice with transgenic *Villin*^{Cre} mice. It is also well-established that the hematopoietic compartment, specifically monocytic and granulocytic cells, also significantly contributes to the progression of experimental colitis and colitis associated cancer.[11] Thus, we crossed our *Nik*$^{fl/fl}$ mice with transgenic *LysM*^{Cre} mice to generate conditional *Nik* deletion in the myeloid compartment. In addition to *Nik*$^{fl/fl}$ mice, we also evaluated canonical NF-κB signaling using previously described *RelA*$^{fl/fl}$ mice, which were also crossed with the *Villin*^{Cre} and *LysM*^{Cre} animals.[38] Cell-type specific deletion of both *Nik* and *RelA* was verified for all mouse lines before studies. All studies were conducted using littermate controls.

To determine the role of NIK in myeloid cells during colitis-associated cancer, *Nik*$^{\Delta MYE}$ (*Nik*$^{fl/fl}$ X *LysM*$^{Cre+}$) and control (*Nik*$^{fl/fl}$ X *LysM*$^{Cre-}$) mice were treated with AOM+DSS. During the extent of the AOM+DSS model, there was no significant variation in clinical score (Figure 6*B*). Although histopathologic features were consistent with increased DSS-induced GI inflammation and colon tumorigenesis, no significant differences were observed between genotypes (Figure 6*C*). Likewise, at necropsy, we did not observe significant differences in polyp sizes or numbers between the *Nik*$^{\Delta MYE}$ and control mice (Figure 6*D* and *E*). Conversely, AOM+DSS studies were also conducted with the *Nik*$^{\Delta CEC}$ (*Nik*$^{fl/fl}$ X *Villin*$^{Cre+}$) and control mice (*Nik*$^{fl/fl}$ X *Villin*$^{Cre-}$) (Figure 6*F*–*M*). Although both the *Nik*$^{\Delta CEC}$ and control mice demonstrated increased clinical scores with each round of DSS, the *Nik*$^{\Delta CEC}$ animals demonstrated significantly increased clinical parameters associated with disease progression at each round of DSS, including changes in behavior, fecal consistency, blood in stool, and weight loss (Figure 6*F*). On necropsy, histopathology assessments revealed that both genotypes of mice demonstrated similar severity of experimental colitis, including immune cell infiltration and an overall IBD Index score (Figure 6*G* and *H*). However, the *Nik*$^{\Delta CEC}$ mice demonstrated significantly increased histopathologic features associated with CRC, including hyperplasia and dysplasia (Figure 6*H*). Consistent with the histology grading, we also observed significant increases in polyp number in the *Nik*$^{\Delta CEC}$ mice compared with the control animals, with no significant differences in polyp size (Figure 6*I*–*K*). Grossly, in addition to the polyps being more numerous in the *Nik*$^{\Delta CEC}$ mice, they also extended up to the transverse colon from the cecum to the rectum (Figure 6*K*). Conversely, polyps in the control animals were localized in the distal, descending colon and rectal region (Figure 6*K*), which is more consistent with the AOM+DSS model.[34] All these polypoid lesions were histologically defined as adenocarcinomas that were composed of disorganized, arborizing dysplastic tubules separated by thick fibrovascular stroma, admixed with mononuclear cells (Figure 6*L*). Furthermore, the colons of *Nik*$^{\Delta CEC}$ mice had markedly increased Ki-67, a marker for cellular proliferation, which extended beyond the typical localization within the mid-distal crypt niche, toward the terminally differentiated CEC niche at the top of the crypts (Figure 6*M*).

RelA Augments Colitis-associated Colorectal Cancer Through Myeloid Cells

Because NIK and noncanonical NF-κB signaling attenuate inflammation-driven tumorigenesis through CECs, we subsequently determined the unique, cell-intrinsic role of noncanonical NF-κB in comparison with canonical NF-κB. Prior studies evaluating the canonical NF-κB signaling pathway using RelA conditional-knockout mice in spontaneous intestinal disease and in DSS-based models of experimental colitis have also revealed that loss of epithelial RelA results in deregulated intestinal proliferation and increased inflammation.[38] Here, we sought to expand these prior studies beyond the short-term, acute inflammation

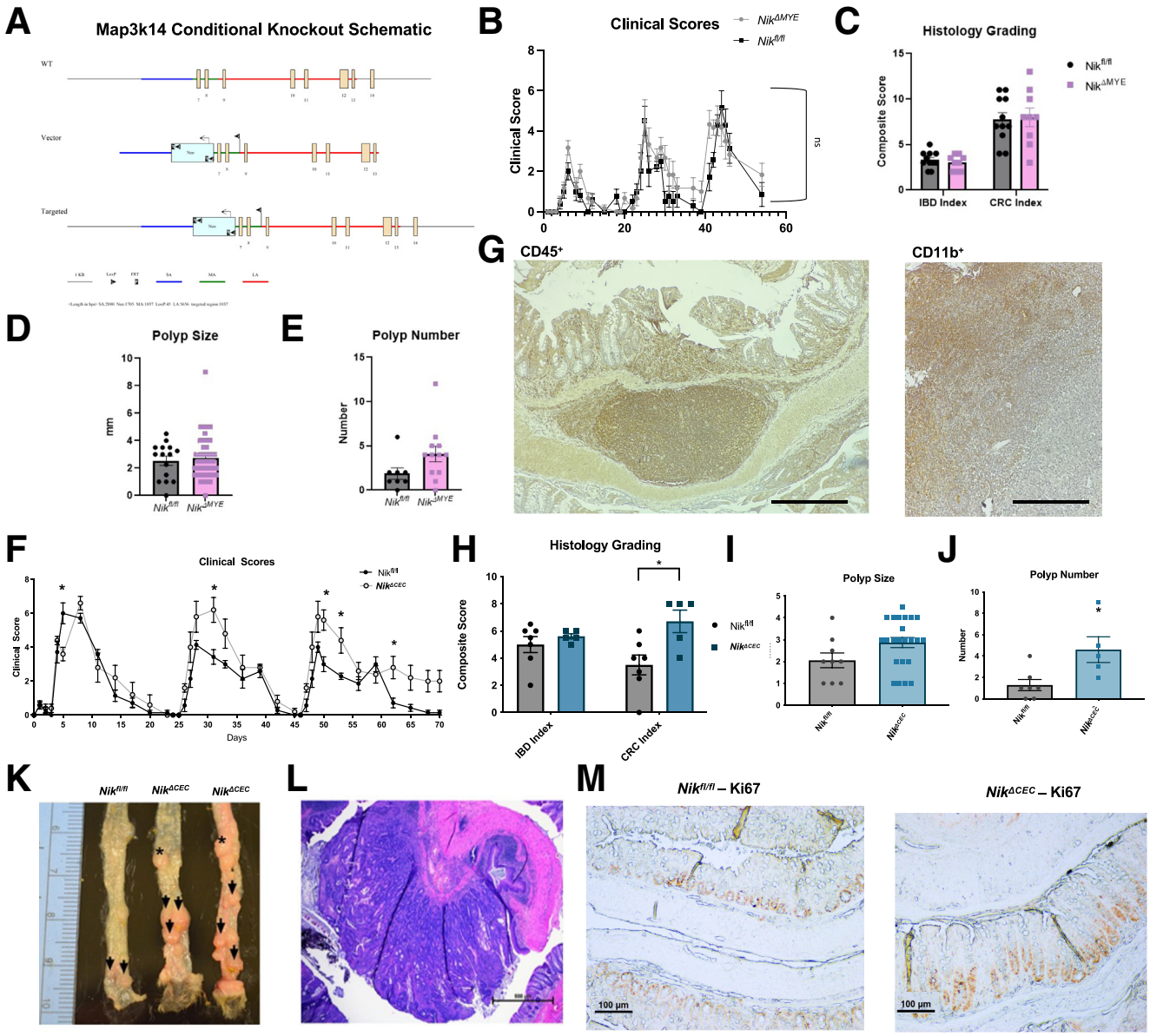

Figure 6. Intestinal epithelial cell specific NIK knockout (*Nik*$^{\Delta CEC}$) mice display increased susceptibility to colorectal tumorigenesis. (*A*) Schematic illustrating the key components of the targeting construct used to insert loxP sites flanking key exons in the kinase domain of the *Map3k14* gene that encodes NIK, ultimately generating *Nik*$^{fl/fl}$ mice. Mice carrying the floxed alleles appear to be phenotypically normal before crossing with Cre expressing animals, with no detrimental effects noted to date. The mice were then subjected to the AOM+DSS model for inflammation-driven tumorigenesis. (*B*) Composite clinical scores were assessed throughout the AOM+DSS model for *Nik*$^{\Delta MYE}$ and *Nik*$^{flox/flox}$ (littermate control) mice. (*C*) Histopathology scoring of *Nik*$^{\Delta MYE}$ and control tissues at completion of the model reflecting experimental colitis (IBD Index) and tumorigenesis (CRC Index). (*D* and *E*) Gross assessments of macroscopic polyps from *Nik*$^{\Delta MYE}$ and control mice measuring (*D*) diameter and (*E*) number of polyps. (*F*) Composite clinical scores from the *Nik*$^{\Delta CEC}$ and *Nik*$^{flox/flox}$ (littermate control) mice. (*G*) Representative histopathology of colonic tissue with immunohistochemistry staining of CD45^{+} cells (*left*) and Cd11b^{+}cells (*right*). For the CD45^{+} image, the lymphoid follicle at the bottom of the image serves as an internal positive control. 10× objective; scale bar represents 100 μm. *Upper portion* of the Cd11b+ image represents positively staining leukocytes in the sero-cellular crust overlying the mucosa. (*H*) Subsequent histopathology scoring of *Nik*$^{\Delta CEC}$ and control tissues at completion of the model. (*I* and *J*) Gross assessments of macroscopic polyps from *Nik*$^{\Delta CEC}$ and control mice measuring (*I*) diameter and (*J*) number of polyps. (*K*) Gross examination of the colon further emphasized the increased tumor burden in the *Nik*$^{\Delta CEC}$ mice. Grossly, polyps were large, raised, smooth to slightly cauliflower-like projections from the mucosa (*arrowheads*) that were typically confined to the distal colon in the *Nik*$^{flox/flox}$ littermates but were found up to the level of the transverse colon in the *Nik*$^{\Delta CEC}$ mice (*asterisks*). (*L*) Histologically, all polyps were determined to represent well-differentiated adenocarcinomas. Histology scale bar = 500 μm. n = 5–7 mice per group. (*M*) Representative images of immunocytochemistry staining for Ki-67 in *Nik*$^{flox/flox}$ (*left*) and *Nik*$^{\Delta CEC}$ (*right*) colons. Increased staining extending toward top of crypt observed in *Nik*$^{\Delta CEC}$ colons. *$P \leq .05$.

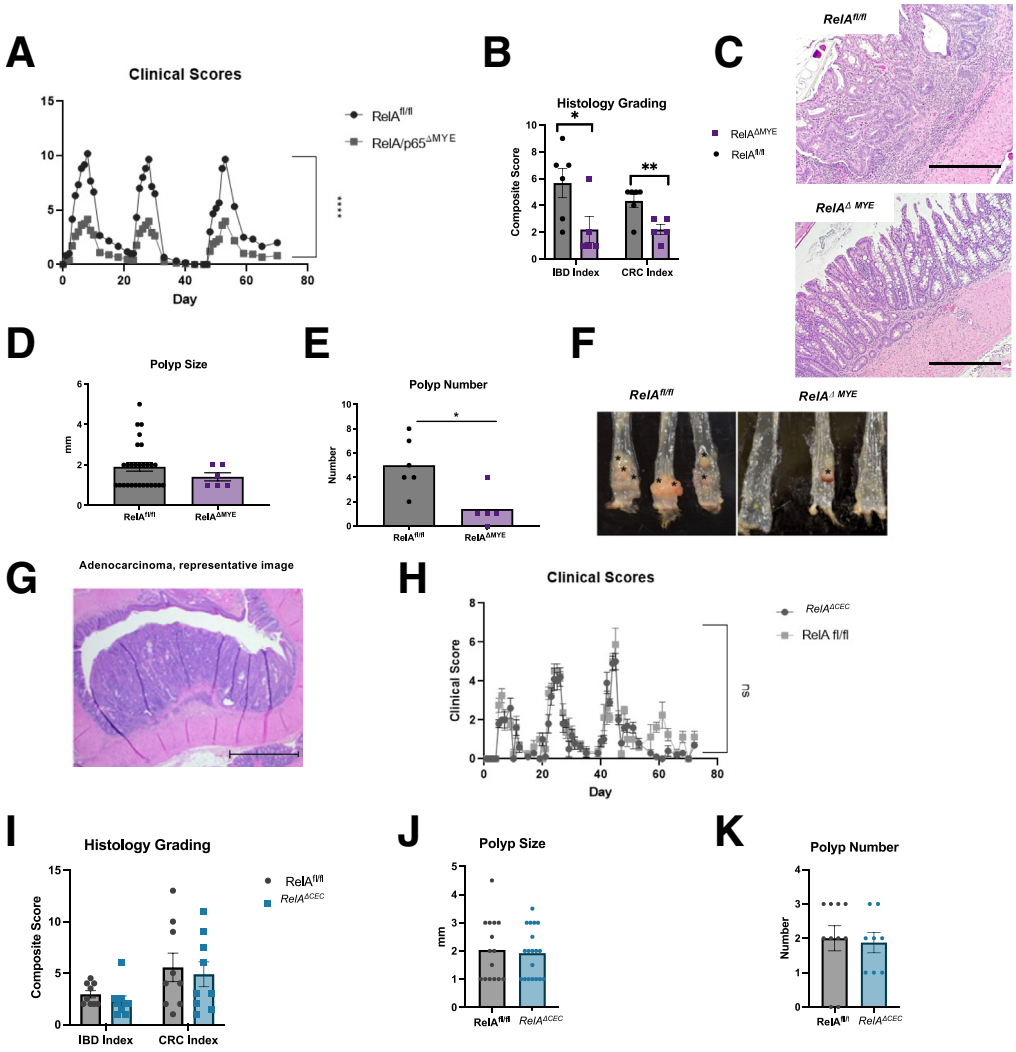

Figure 7. Myeloid cell-specific RelA knockout (*RelA*$^{\Delta MYE}$) mice display attenuated colorectal tumorigenesis. The mice were subjected to the AOM+DSS model of inflammation-driven tumorigenesis. (*A*) Composite clinical scores composed of weight loss, fecal consistency, rectal bleeding, and behavior evaluations were assessed throughout the AOM+DSS model for *RelA*$^{\Delta MYE}$ and *RelA*$^{flox/flox}$ (littermate control) mice. (*B* and *C*) Histopathology scoring of *RelA*$^{\Delta MYE}$ and control tissues at completion of the model reflecting experimental colitis (IBD Index) and tumorigenesis (CRC Index). (*D* and *E*) Gross assessments of macroscopic polyps from *RelA*$^{\Delta MYE}$ and control mice measuring (*D*) diameter and (*E*) number of polyps. (*F*) Gross examination of the colon further emphasized the decrease in tumor burden in the *RelA*$^{\Delta MYE}$ mice. Grossly, polyps from the *RelA*$^{\Delta MYE}$ mice were seldom observed. All polyps in both genotypes were confined to the distal colon (*asterisks*). (*G*) Histologically, all polyps were determined to represent well-differentiated adenocarcinomas. Hematoxylin-eosin, 10×; scale bar = 250 μm. (*H*) Composite clinical scores from the *RelA*$^{\Delta CEC}$ and *RelA*$^{flox/flox}$ (littermate control) mice. (*I*) Histopathology scoring of *RelA*$^{\Delta CEC}$ and control tissues at completion of the model reflecting IBD Index and CRC Index. (*J* and *K*) Gross assessments of macroscopic polyps from *RelA*$^{\Delta CEC}$ and control mice measuring (*J*) diameter and (*K*) number of polyps. Histology scale bar = 500 μm. n = 5–7 mice per group. *$P \leq .05$; **$P \leq .01$.

model and evaluate the cell-type specific role of canonical NF-κB signaling in the context of inflammation-driven tumorigenesis. Thus, the *RelA*$^{\Delta MYE}$ (*RelA*$^{fl/fl}$ X *LysM*$^{Cre+}$) and control (*RelA*$^{fl/fl}$ X *LysM*$^{Cre-}$) mice were treated with AOM+DSS. Unlike the *Nik*$^{\Delta MYE}$ mice, the *RelA*$^{\Delta MYE}$ mice were significantly protected from the development of colitis-associated cancer (Figure 7*A*–*G*), which recapitulates findings described in conditional IKK β knockout mice.[11] Specifically, these animals demonstrated significantly improved clinical scores throughout each round of DSS-driven colon inflammation compared with the control animals (Figure 7*A*). Histopathology evaluation revealed increased features consistent with colitis in both sets of mice; however, the *RelA*$^{\Delta MYE}$ mice had a significantly attenuated IBD and CRC indexes compared with the control animals (Figure 7*B*). This was predominantly associated with reduced inflammation in the colon (Figure 7*C*). Gross assessment of the colons revealed significantly reduced numbers of polyps, which were also smaller in size in the *RelA*$^{\Delta MYE}$ mice compared with the controls (Figure 7*D*–*F*). In both sets of mice, these polypoid lesions were histologically defined as adenocarcinomas (Figure 7*G*). However, our

results differed in $RelA^{\Delta CEC}$ when compared with those described in conditional IKK β knockout mice.[11] To elaborate, in our $RelA^{\Delta CEC}$ model, we did not observe any significant differences in clinical progression between the $RelA^{\Delta CEC}$ and their respective control mice (Figure 7*H*). This was confirmed histopathologically in the IBD and CRC indexes (Figure 7*I*) and grossly with similar sizes and numbers of macroscopic polyps (Figure 7*J* and *K*). These results suggest that intestinal RelA downstream of IKK β is dispensable for inflammation-induced CRC.

Loss of NIK Compromises CEC Differentiation and Regeneration

Deletion of NIK in epithelial cells increased susceptibility to inflammation-induced CRC. To better characterize the transcriptional impact of NIK loss in CECs (Figure 6), we next performed Clariom S transcriptome analysis of $Nik^{\Delta CEC}$ lesion tissue (LT) and $Nik^{\Delta CEC}$ non-lesion "healthy" tissue (HT) after AOM+DSS (Figure 6). We also did not observe any significant differences in the transcription profiles between $Nik^{\Delta CEC}$ HT and control mouse HT at baseline (data not shown). We identified 19 genes related to NF-κB signaling that were significantly up-regulated in $Nik^{\Delta CEC}$ LT compared with adjacent HT, including several inflammatory cytokines and chemokines (Figure 8*A*). We also identified one gene (*Tnfrsf11A*) that was significantly down-regulated in the $Nik^{\Delta CEC}$ LT compared with adjacent HT (Figure 8*A*). We also identified 25 additional up- and down-regulated genes that were altered in $Nik^{\Delta CEC}$ LT compared with HT (Figure 8*B* and *C*). These genes were generally found to contribute to biological functions associated with intestinal barrier function and host-bacteria interactions by Gene Ontology analysis (Figure 8*D*). The data also suggested altered regulation of epithelial cell proliferation in $Nik^{\Delta CEC}$ LT compared with control $Nik^{fl/fl}$ LT (Figure 8*E*).

Transcriptome analysis further revealed altered gene expression related to stem cell function (Figure 8*F*), epithelial cell differentiation (Figure 8*G*), and epithelial cell development (Figure 8*H*) in $Nik^{\Delta CEC}$ LT compared with HT. We then looked back at transcriptome analysis from whole-body $Nik^{-/-}$ mice for comparison. These results also revealed diminished regulation of cancer pathways (especially cellular senescence) and apoptosis in the $Nik^{-/-}$organoids in vitro (Figure 8*I* and *J*). Reciprocally, $Nik^{-/-}$organoids were characterized by up-regulation of genes related to wound healing, including 796.99-fold change up-regulation of the ECR remodeling enzyme gene *Mmp7* (Figure 8*K*). Together, these data may suggest that epithelial cells in the $Nik^{\Delta CEC}$ and $Nik^{-/-}$ mice fail to reach typical maturation given improper differentiation signaling, may live longer, or may impart a "stem-like" phenotype to the overall epithelial cells associated with diseased tissue in vivo.

Discussion

Altogether, our data suggest that CEC-associated NIK protects the colon from tumorigenesis, likely through the regulation of noncanonical NF-κB signaling and its effects on CEC development. We have previously discussed how NIK contributes to the development of cancer through multiple mechanisms and cell types. However, the role of NIK in the gut and its contribution to CRC are both complex and not yet well-defined. Early studies by our research team found that loss of negative regulation of NIK, coupled with increased p100 processing to p52 and reduced TRAF3 signaling, increased GI inflammation and tumorigenesis in colitis associated cancer (CAC) models.[5] This is consistent with other findings associated with NIK signaling in mucosal dendritic cells where the loss of NIK signaling attenuated colitis induction.[10]

Our current work demonstrates that the role of NIK in attenuation of CRC lies in its effects on CSC and CEC development, proliferation, and maturation. Our in vitro data show that in the absence of NIK and noncanonical NF-κB signaling, crypts exhibit decreased Ki-67 staining, suggesting lowered proliferative capacity in vitro (Figure 3*A* and *B*). Interestingly, we noted enhanced Ki-67 staining in the crypt region after AOM+DSS treatment of $Nik^{\Delta CEC}$ in vivo (Figure 6*M*), suggesting hyperproliferation after inflammatory and carcinogenic stimuli when compared with wild-type counterparts. Furthermore, the elongation of the crypts noted in whole-body $Nik^{-/-}$ mice was also associated with a mature epithelial cell signature and altered tumor development, apoptotic, cancer, and wound healing signatures when compared with wild-type counterparts in vitro (Figure 3*D*–*F* and 8*I*–*K*). This is further supported by the reduced *Lgr5* expression in the crypt preps from the $Nik^{-/-}$ mice (Figure 3*C*) in vitro as *Lgr5* may be important in regulating stemness in CECs and CSCs.[39] Furthermore, in the absence or suppression of *Lgr5* and a range of other stem cell markers, mature enterocytes have been previously reported to gain plasticity.[40] This newly acquired plasticity can result in terminally differentiated cells to regain "stem-like" features such as accelerated growth.[40] Overall, given the altered proliferative capacity, apoptotic potential, skewed maturation, and overall dysregulated activity within amplifying zones of crypts, it appears that NIK disruption within the colonic epithelium leads to enhanced dysplastic potential throughout the villus. This change is not clinically or morphologically apparent under normal, homeostatic conditions (Figure 4*A* and *B*). However, after chronic inflammatory stimuli or on exposure to carcinogens as demonstrated in our in vivo models, it appears that the attempted regeneration and repair of the colonic mucosa lead to shortening of the colon and compounded dysplasia (torturous mucosa and loss of goblet cells, for example) that accrues in the colonic epithelium; thus, predisposing the animals to neoplastic transformation of the colonic tissue (Figure 4*F*–*J*).

Not only did loss of NIK affect the mucosa within the colon, but it also skewed the associated microbiome with several bacterial species that are commonly associated with dysbiosis (Figure 5). In general, the microbiome appears to play a complex and multifaceted role in gut health in relation to immune cell activation, maintenance of the gut barrier, and nutrient processing.[41] In some instances, it is also unclear whether the microbiome causes inflammation

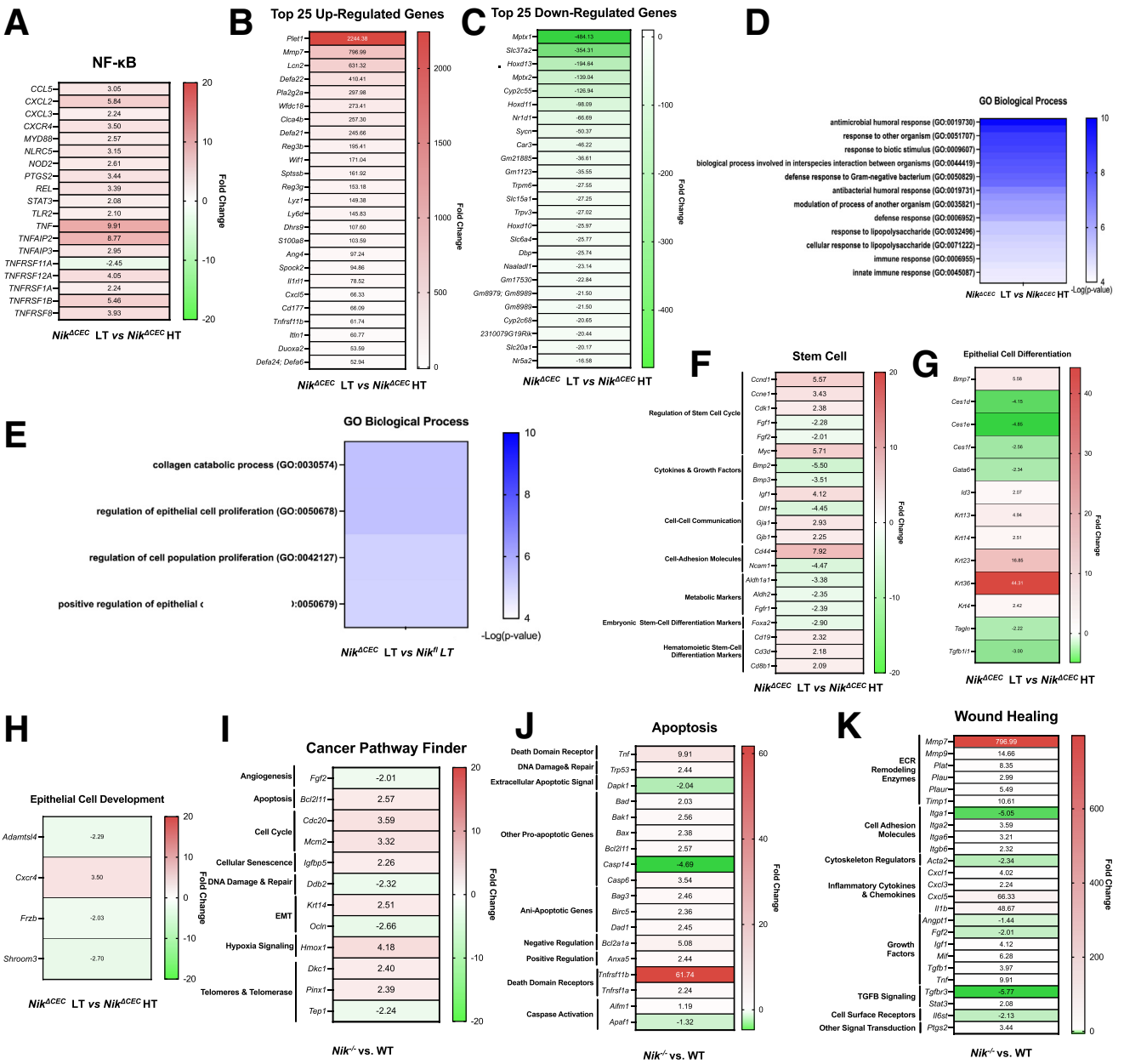

Figure 8. Gene expression signature after loss of NIK reveals altered differentiation-regeneration profile. Gene expression profiles for (*A*) NF-κB signaling, (*B*) top-25 up-regulated genes, and (*C*) top 25 down-regulated genes. (*D* and *E*) Altered biological functions predicted by Gene Ontology (GO) given unique transcriptome profiles. (*D*) $Nik^{\Delta CEC}$ lesions are predicted to have increased defense responses to bacterial infection. (*E*) $Nik^{\Delta CEC}$ lesion compared with $Nik^{fl/fl}$ lesion tissue predicted to have altered regulation of epithelial cell proliferation. Gene expression profiles for (*F*) stem cell functions, (*G*) epithelial cell differentiation, (*H*) epithelial cell development, (*I*) cancer pathways, (*J*) apoptosis, and (*K*) wound healing. n = 3 representative mice/group selected from AOM+DSS study performed in Figure 6*F–M* or crypt organoid study in Figure 3 for transcriptome analysis. Significant values ≥2 (*red*) and ≤2 (*green*) reported as fold-change. Values that did not reach significance (*white*) in heatmap.

leading to gut pathologies, or whether it is altered as a consequence of the inflammation induced by a dysregulated immune system.[41] However, this conundrum reveals that there is indeed crosstalk between the two. In our $Nik^{-/-}$ mice at baseline and despite the altered microbiome, we did not see clinical signs associated with dysbiosis (such as diarrhea or inflammation in the mucosa at baseline) when compared with wild-type counterparts. If the immune system in these mice is "conditioned" to the altered microbiota in health, then perhaps there is no resultant inflammation at baseline. However, we postulate that the skewing of this microbiome may simply exacerbate the inflammatory stimulus that is initiated with DSS administration. The resultant robust inflammation likely drives epithelial dysplasia that leads to

malignant transformation. There is further work to test this hypothesis in future studies.

Interestingly, noncanonical NF-κB activity within the myeloid compartment appeared dispensable for IBD and CRC indexes, as well as polyp formation (Figure 6*B–E*). This is in contrast to canonical signaling in myeloid cells, because the *RelA*$^{\Delta MYE}$ mice have also been previously evaluated in the DSS model.[42] These animals demonstrate attenuated experimental colitis linked to altered expression of IL-6, Ccl11, and calprotectin in the DSS-treated colons.[42] Although this study used acute DSS to model experimental colitis in the *RelA*$^{\Delta MYE}$ animals, it did not evaluate relapsing remitting colitis or cancer development. Similar to the findings from the acute DSS study,[38] we observed that the contribution of the myeloid compartment (macrophages and granulocytes) to chronic inflammation associated with CRC development was favorable in *RelA*$^{\Delta MYE}$ mice, because we noted significantly decreased polyp formation (Figure 7*A–F*). This suggests a protective role for the canonical pathway in myeloid cells during chronic inflammation and subsequent tumor development.

Previous studies have also used the *RelA*$^{\Delta CEC}$ mice in the DSS model of acute experimental colitis to assess the role of canonical NF-κB signaling in the colonic epithelium.[38] These animals were found to be more susceptible to a single round of acute DSS, with increased proliferation, sustained epithelial cell apoptosis, and decreased animal survival.[38] In addition, other studies have revealed that activation of canonical NF-κB in the crypt stem cell niche appears to enhance Wnt signaling to promote the de-differentiation of the CECs, thereby promoting tumorigenesis in the gut.[8] Interestingly, our study of chronic inflammation and CRC development in *RelA*$^{\Delta CEC}$ mice revealed no significant alterations in IBD or CRC indexes, and this did not alter polyp size or number when compared with wild-type counterparts (Figure 7*H–K*). This suggests that canonical NF-κB activity does not intrinsically affect the development of epithelial lesions within the colon. Overall, our data provide an intriguing contrast between the contribution of NIK/noncanonical NF-κB and RelA/canonical NF-κB signaling in the CEC and myeloid compartments during CAC development.

The increased inflammation and tumor susceptibility in the *Nik*$^{\Delta CEC}$ mice (Figure 6*F–L*) are consistent with altered CEC turnover (Figure 6*M*), which likely favors accumulation of CECs with dysplastic features and resistance to apoptosis resulting in subsequent tumorigenesis. Reduced CEC turnover has been reported in acute experimental colitis models using a different conditional NIK deficient mouse line, whereby loss of NIK is mediated by tamoxifen-inducible Cre recombinase driven by the villin promoter (*Nik*$^{F/F;VilERT2Cre}$).[21] Similar to our findings reported here, these CEC-deficient mice demonstrated enhanced inflammation after a single round of 2% DSS for 7 days.[21] This was shown to be p52 dependent, indicating that the mechanism was associated with dysregulated noncanonical NF-κB signaling, with additional studies revealing a role for RANK signaling upstream of NIK.[21] IL-17 mediated immunoglobulin A production appeared to be protective in this model and attenuated the observed phenotype.[21] This same study found that constitutive expression of NIK and noncanonical NF-κB signaling also increased susceptibility to inflammatory injury through inducing M-cell differentiation and chronic increases in IL-17A.[21] Mechanistically, NIK was found to regulate Microfold cell (M-cell) maintenance and differentiation, impacting the function of the intestinal lymphoid follicles.[21] M-cells are specialized CECs that regulate luminal microbiota and dietary antigen sampling in the gut. Although this study is one of the most comprehensive assessments of NIK and noncanonical NF-κB signaling in the gut to date, the work is specifically focused on GI inflammation over a short duration in an acute model. The cancer studies presented in the current work do not specifically evaluate the M-cells. However, it is likely that this mechanism contributes to the in vivo protective effects of NIK in the CAC studies. It is important to note that the crypt and organoid data included here indicate that NIK is contributing to other mechanisms in the mature enterocytes beyond the M-cells. For example, M-cells are not part of the organoids shown in Figure 3. Organoids require RANKL and other specific factors added exogenously, which were not included here, to differentiate and include M-cells.[43] Thus, the truncated development of the *Nik*$^{-/-}$ organoids is associated with an M-cell independent mechanism.

In conclusion, we show that NIK and non-canonical NF-κB signaling plays a protective role in human patients and in mouse models of inflammation-driven colon tumorigenesis. Our studies using novel *Nik*$^{\Delta CEC}$ conditional-knockout mice show that this protective mechanism is driven through the CEC compartment. This contrasts with RelA and the canonical NF-κB signaling pathway, which promotes CAC driven tumor development through the modulation of inflammation driven through the myeloid compartment. Mechanistically, our data support altered CEC development in the *Nik*$^{-/-}$ and *Nik*$^{\Delta CEC}$ mice, whereby CEC regeneration is dysregulated, allowing elongated crypts that are the result of faulty apoptosis and altered proliferation/differentiation in CECs to contribute to tumorigenesis. Specifically, the accumulation of dysplastic and neoplastic colonocytes is predicted to arise from mutations within CSCs in the colonic crypts. These mutations likely arise secondary to increased inflammation and environmental insults in the colon. NIK appears to protect against this process by regulating CEC and CSC turnover along the crypt length. Future work may include further investigation of CEC turnover after loss of NIK in contributing to better characterization of this phenotype.

Methods

Human Specimens

CRC biopsy samples were collected from 6 patients and 6 controls. Control specimens were from endoscopically/histologically unaffected tissue in patients presenting for conditions other than IBDs or CRC. All sections were confirmed by a pathologist to contain either neoplasia (CRC) or lack of histologic change (control). RNA was extracted from CRC tissue preserved as 50-μm sections of formalin-fixed paraffin-embedded tissue and RNAlater-preserved control

tissue. Extractions were performed using the Qiagen AllPrep kit according to manufacturer's protocols.

Human Metadata Analysis

Using the Oncomine Platform (www.oncomine.org), we identified microarray studies of human CRC patients and evaluated noncanonical gene expression in biopsy tissue. Relative expression was reported as log-transformed median-centered data used in the following data sets (CRC/control): Gaedcke (65/65),[44] Skrzypczak (81/24),[45] Hong (70/12),[46] TCGA colon cancer (215/22),[47] Kaiser (100/5),[48] Graudens (18/12),[49] Ki (50/28),[50] Gaspar (56/22),[51] Notterman (18/18),[52] and Sabates-Bellver (32/32).[53] Figures were created using GraphPad Prism software v.7, and statistical significance was determined using the unpaired Mann-Whitney *U* test. Significance was set at $P \leq .05$.

Experimental Animals

Conventional *Map3K14* deficient mice ($Nik^{-/-}$) have been previously described and were provided by Amgen and Dr Vanessa Redecke (St. Jude).[4] The *Map3K14* flox mice ($Nik^{fl/fl}$) are novel and were generated by the PI and Ingenious Targeting Laboratory following general protocols as previously described and outlined in Figure 7*A*.[54] The $RelA^{fl/fl}$ mice have been previously described and were provided by Dr Al Baldwin (UNC Chapel Hill).[38] Apc^{min} mice (*C57BL/6J-ApcMin/J*) were commercially acquired (Jackson Laboratory). Mice carrying floxed alleles were crossed with transgenic mice that express Cre recombinase under the control of either the *Villin* promoter ((*B6.Cg-Tg(Vil1-cre)1000Gum/J* (*Villin-Cre)*) or the *LysM* promoter ((*B6.129P2-Lyz2tm1(cre)Ifo/J (LysM-cre)*), resulting in CEC or myeloid cell specific deletions, respectively. *Villin-Cre* and *LysM-Cre* mice were commercially acquired (Jackson Laboratories). Gene deletion was confirmed before and/or after all studies using polymerase chain reaction genotyping and Western blot for either NIK or RelA in selected mouse tissues. All animals were maintained as breeder colonies at Virginia Tech's vivarium under specific pathogen-free conditions for the duration of the study. All animals were maintained on the C57Bl/6 background. All animals were fed ad libitum with standard rodent chow (Research Diets) and maintained in a 12-hour light/dark cycle. For all studies/experiments, littermate controls were used. Control and mutant animals were housed separately.

Induction of Colitis and Inflammation-driven Tumor Progression

Acute experimental colitis was induced by exposing mice to a single cycle of 5% DSS (MP Biomedicals; Affymetrix) for 5 days and harvested on day 8 as previously described.[33] Relapsing, remitting experimental colitis was induced by exposing the mice to 3 cycles of 2.5% DSS (MP Biomedicals, Affymetrix) as previously described.[55] To induce inflammation-driven colitis-associated cancer, mice were given 1 intraperitoneal injection (10 mg/kg body weight) of the mutagen AOM (Sigma-Aldrich), followed by 3 DSS exposures (2.5%) as previously described.[5] For all studies, mice were killed and characterized at the planned end of the study (up to 60 days) or when the animals were moribund. Disease progression was determined by the change in body weight, the presence of rectal bleeding, and stool consistency. Parameters were scored and averaged to generate a semiquantative clinical score as described.[55,56] Mice were euthanized by carbon dioxide narcosis, followed by cervical dislocation. Colon length was measured on completion of each study. Because of well-defined sex differences in response to DSS,[57] only male mice were used in the colitis and colitis-associated cancer studies.

Macroscopic Polyp Analysis and Histopathology

The entire colon was removed, flushed, and opened longitudinally for assessing macroscopic polyp formation as previously described.[5,33,55,58] Polyps were identified by a trained investigator with a dissecting microscope. For histopathology, the colons were Swiss rolled and fixed in 10% buffered formalin, paraffin embedded, processed routinely, sectioned at 5 μm, and stained with H&E. Grading was performed using a standard scheme including both inflammatory and hyperplasia parameters.[59]

Crypt Harvest and Enteroid Culture

Colonic crypts were harvested from mice as previously described.[60] Organoids were created from isolated colonic crypts following established protocols.[60] Diameter was measured from randomly selected organoids from multiple wells by a blinded investigator. For growth tracking pictures, the same organoids were measured over time by marking the outside of the plate to consistently identify the same organoid.

Immunohistochemistry and Quantification

Smears for immunocytochemistry were made by using histology sections of Swiss rolled colonic preparations or by placing a drop of concentrated crypt suspension on a frosted microscope slide and allowed to air-dry. Histology samples and smears were then fixed in 4% paraformaldehyde for 10 minutes and rinsed with 1× phosphate-buffered saline. Enzymatic antigen retrieval was performed using a 0.5% trypsin solution in distilled water. Immunocytochemistry was performed according to the manufacturer's protocol using the Pierce IHC kit and an anti-mouse Ki-76 antibody (CST Product #12202) at a 1:1000 dilution, anti-mouse CD45 antibody (Abcam Product #ab10558) at 1:200 dilution, or anti-mouse CD11b antibody (Abcam Product #ab133357) at 1:4000 dilution. Image quantification was performed using ImageJ.

Real-Time Quantitative Polymerase Chain Reaction

RNA was quantified via Nanodrop and converted to cDNA using a Thermo Fisher Hi Capacity cDNA kit. Pathway focused gene expression was evaluated using custom noncanonical NF-κB signaling from Superarray Platforms (Qiagen). Individual real-time polymerase chain reaction was performed using Taqman primers for specific human and

mouse targets with 18s as an internal control. All studies were evaluated on an ABI 7500 Fast Block Thermocycler. Fold change was calculated using the ΔΔCt method,[61] and all changes were log-transformed. Statistics were performed using GraphPad Prism v. 7 and the unpaired Mann-Whitney *U* test. Significance was set at $P > .05$.

Clariom S Microarray

Mouse RNA specimens were prepared for Clariom S Assays following vendor guidelines (Thermo Fisher). The Clariom S Assay is microarray based and provides extensive coverage of >20,000 well-annotated genes. Briefly, cDNA was generated from RNA, quality and yield were verified following RNase H treatment, and loaded onto GeneChipMouse Transcriptome Array 2.0. Cartridge array hybridization was conducted on the GeneChip Instrument, with target hybridization, washing, staining, and scanning. Data were analyzed using the Transcriptome Analysis Console (TAC) 4.0. Further high-resolution pathway analysis was conducted using IPA (Qiagen) and CompBio (Canopy Bioscience) software. Findings were also compared with results from publicly accessible microarray and RNAseq meta-analysis. All differentially expressed genes were reported as fold-change and considered significant if ≥2, ≤-2.

Enzyme-linked Immunosorbent Assay and Immunoblots

All tissues were processed as previously described.[5] All enzyme-linked immunosorbent assays used commercial kits and were conducted following manufacturer's procedures. For immunoblots, a total of 30 μg of protein from each sample was separated by sodium dodecyl sulfate-polyacrylamide gel electrophoresis with 4%-12% NuPAGE Bis-Tris gels (Invitrogen), transferred, and incubated overnight with the respective antibodies. Anti-actin-HRP (sc-1615 HRP) (Santa Cruz Biotechnology) was used as a loading control in all studies.

16S rRNA Gene Sequencing and Bacterial Community Analysis

Colonic contents were collected aseptically from the entire colon length of mice into a sterile microcentrifuge tube and immediately frozen at −80°C. Bacterial DNA was extracted using the QIAamp DNA Stool Mini Kit. Twenty ng DNA from each sample was used to generate the libraries for 16s rDNA sequencing on an Illumina Miseq. Each sample had more than 200,000 reads, and 99% of reads passed Q20. After QC and trimming the adaptors, mothur (http://www.mothur.org/) was used to analyze the data. Paired-end reads were joined and mapped to the Greengenes 13.8 release database. Operational taxonomic units were picked against Greengenes database, using a 97% similarity threshold. To avoid the different sequencing depth, all samples were normalized to the same number of reads in the following analysis. Lefse (https://huttenhower.sph.harvard.edu/galaxy/) was used to compare the different bacteria abundance in knockout and wild-type mice. A diversity was calculated with 95% confidence interval. Heatmap plots with bacterial operational taxonomic units were created with more than 1000 reads.

Graphical Illustrations

Graphical illustrations and schematics were generated using Biorender.com.

Statistics

Data were analyzed using GraphPad Prism, version 7 (GraphPad Software, Inc, San Diego, CA). The Student two-tailed *t* test was used for comparison of 2 experimental groups. Multiple comparisons were performed using one-way and two-way analysis of variance where appropriate. Changes were identified as statistically significant if *P* was less than .05. Mean values were reported together with the standard error of the mean or standard deviation, as appropriate. All studies were repeated at least 3 independent times with representative data from single experiments shown. All authors had access to the study data and had reviewed and approved the final manuscript.

Study Approval

All human studies were conducted following Duke University and Virginia Tech's Institutional Review Board guidelines. Written informed consent was received from patients before participation. All animal studies were conducted in accordance with Virginia Tech's IACUC guidelines and the NIH Guide for the Care and Use of Laboratory Animals.

References

1. McDaniel DK, Eden K, Ringel VM, et al. Emerging Roles for Noncanonical NF-kappaB Signaling in the Modulation of Inflammatory Bowel Disease Pathobiology. Inflamm Bowel Dis 2016;22(9):2265–2279.
2. Nguyen VQ, Eden K, Morrison HA, et al. Noncanonical NF-kappaB Signaling Upregulation in Inflammatory Bowel Disease Patients is Associated With Loss of Response to Anti-TNF Agents. Front Pharmacol 2021;12:655887.
3. Eden K, Rothschild DE, McDaniel DK, et al. Noncanonical NF-kappaB signaling and the essential kinase NIK modulate crucial features associated with eosinophilic esophagitis pathogenesis. Dis Model Mech 2017;10(12):1517–1527.
4. Häcker H, Chi L, Rehg JE, et al. NIK prevents the development of hypereosinophilic syndrome-like disease in mice independent of IKKalpha activation. J Immunol 2012;188(9):4602–4610.
5. Allen IC, Wilson JE, Schneider M, et al. NLRP12 suppresses colon inflammation and tumorigenesis through the negative regulation of noncanonical NF-kappaB signaling. Immunity 2012;36(5):742–754.
6. Myant KB, Cammareri P, McGhee EJ, et al. ROS production and NF-kappaB activation triggered by RAC1 facilitate WNT-driven intestinal stem cell proliferation and

colorectal cancer initiation. Cell Stem Cell 2013; 12(6):761–773.
7. Qin M, Zhang J, Xu C, et al. Knockdown of NIK and IKKbeta-Binding Protein (NIBP) Reduces Colorectal Cancer Metastasis through Down-Regulation of the Canonical NF-kappaBeta Signaling Pathway and Suppression of MAPK Signaling Mediated through ERK and JNK. PLoS One 2017;12(1):e0170595.
8. Schwitalla S, Fingerle AA, Cammareri P, et al. Intestinal tumorigenesis initiated by dedifferentiation and acquisition of stem-cell-like properties. Cell 2013;152(1-2):25–38.
9. Jang H, Park S, Kim J, et al. The Tumor Suppressor, p53, Negatively Regulates Non-Canonical NF-kappaB Signaling through miRNAInduced Silencing of NF-kappaB-Inducing Kinase. Mol Cells 2020;43(1):23–33.
10. Jie Z, Yang J-Y, Gu M, et al. NIK signaling axis regulates dendritic cell function in intestinal immunity and homeostasis. Nat Immunol 2018;19(11):1224–1235.
11. Greten FR, Eckmann L, Greten TF, et al. IKKbeta links inflammation and tumorigenesis in a mouse model of colitis-associated cancer. Cell 2004;118(3):285–296.
12. Senftleben U, Cao Y, Xiao G, et al. Activation by IKKalpha of a second, evolutionary conserved, NF-kappa B signaling pathway. Science 2001;293(5534):1495–1499.
13. Shih VF, Tsui R, Caldwell A, et al. A single NFkappaB system for both canonical and non-canonical signaling. Cell Res 2011;21(1):86–102.
14. Madge LA, May MJ. Classical NF-kappaB activation negatively regulates noncanonical NF-kappaB-dependent CXCL12 expression. J Biol Chem 2010; 285(49):38069–38077.
15. Wharry CE, Haines KM, Carroll RG, et al. Constitutive non-canonical NFkappaB signaling in pancreatic cancer cells. Cancer Biol Ther 2009;8(16):1567–1576.
16. Yin L, Wesche H, Arthur CD, et al. Defective lymphotoxin-beta receptor-induced NF-kappaB transcriptional activity in NIK-deficient mice. Science 2001; 291(5511):2162–2165.
17. Miyawaki S, Nakamura Y, Hirotsugu S, et al. A new mutation, aly, that induces a generalized lack of lymph nodes accompanied by immunodeficiency in mice. Eur J Immunol 1994;24(2):429–434.
18. Matsushima A, Kaisho T, Rennert PD, et al. Essential role of nuclear factor (NF)-kappaB-inducing kinase and inhibitor of kappaB (IkappaB) kinase alpha in NF-kappaB activation through lymphotoxin beta receptor, but not through tumor necrosis factor receptor I. J Exp Med 2001;193(5):631–636.
19. Koni PA, Sacca R, Lawton P, et al. Distinct roles in lymphoid organogenesis for lymphotoxins alpha and beta revealed in lymphotoxin beta-deficient mice. Immunity 1997;6(4):491–500.
20. Fütterer A, Mink K, Luz A, et al. The lymphotoxin beta receptor controls organogenesis and affinity maturation in peripheral lymphoid tissues. Immunity 1998;9(1):59–70.
21. Ramakrishnan SK, Zhang H, Ma X, et al. Intestinal noncanonical NFkappaB signaling shapes the local and systemic immune response. Nat Commun 2019; 10(1):660.
22. Lich JD, Williams KL, Moore CB, et al. Monarch-1 suppresses non-canonical NF-kappaB activation and p52-dependent chemokine expression in monocytes. J Immunol 2007;178(3):1256–1260.
23. Kim JY, Morgan M, Kim D-G, et al. TNFalpha induced noncanonical NF-kappaB activation is attenuated by RIP1 through stabilization of TRAF2. J Cell Sci 2011; 124(Pt 4):647–656.
24. Hu H, Brittain GC, Chang J-H, et al. OTUD7B controls non-canonical NF-kappaB activation through deubiquitination of TRAF3. Nature 2013;494(7437):371–374.
25. Nottingham LK, Yan CH, Yang X, et al. Aberrant IKKalpha and IKKbeta cooperatively activate NF-kappaB and induce EGFR/AP1 signaling to promote survival and migration of head and neck cancer. Oncogene 2014; 33(9):1135–1147.
26. Jin J, Hu H, Haiyan SL, et al. Noncanonical NF-kappaB pathway controls the production of type I interferons in antiviral innate immunity. Immunity 2014;40(3):342–354.
27. Walsh NC, Waters LR, Fowler JA, et al. LKB1 inhibition of NF-kappaB in B cells prevents T follicular helper cell differentiation and germinal center formation. EMBO Rep 2015;16(6):753–768.
28. Piao W, Xiong Y, Famulski K, et al. Regulation of T cell afferent lymphatic migration by targeting LTbetaR-mediated non-classical NFkappaB signaling. Nat Commun 2018;9(1):3020.
29. Fagarasan S, Shunkura R, Kamata T, et al. Alymphoplasia (aly)-type nuclear factor kappaB-inducing kinase (NIK) causes defects in secondary lymphoid tissue chemokine receptor signaling and homing of peritoneal cells to the gut-associated lymphatic tissue system. J Exp Med 2000;191(9):1477–1486.
30. Schatoff EM, Leach BI, Dow LE. Wnt Signaling and Colorectal Cancer. Curr Colorectal Cancer Rep 2017; 13(2):101–110.
31. Yilmaz ZB, Weih DS, Sivakumar V, et al. RelB is required for Peyer's patch development: differential regulation of p52-RelB by lymphotoxin and TNF. EMBO J 2003; 22(1):121–130.
32. Shinkura R, Kitada K, Matsuda F, et al. Alymphoplasia is caused by a point mutation in the mouse gene encoding Nf-kappa b-inducing kinase. Nat Genet 1999;22(1):74–77.
33. Allen IC, TeKippe EM, Woodford R-MT, et al. The NLRP3 inflammasome functions as a negative regulator of tumorigenesis during colitis-associated cancer. J Exp Med 2010;207(5):1045–1056.
34. Neufert C, Becker C, Neurath MF. An inducible mouse model of colon carcinogenesis for the analysis of sporadic and inflammation-driven tumor progression. Nat Protoc 2007;2(8):1998–2004.
35. Lopetuso LR, Scaldaferri F, Petito V, et al. Commensal Clostridia: leading players in the maintenance of gut homeostasis. Gut Pathogens 2013;5(1):23.
36. Varon C, Azzi-Martin L, Khalid S, et al. Helicobacters and cancer, not only gastric cancer? Seminars in Cancer Biology 2022;86:1138–1154.
37. Jakobsson HE, Rodríguez-Piñero AM, Schütte A, et al. The composition of the gut microbiota shapes the colon mucus barrier. EMBO Rep 2015;16(2):164–177.

38. Steinbrecher KA, Harmel-Laws E, Sitcheran R, et al. Loss of epithelial RelA results in deregulated intestinal proliferative/apoptotic homeostasis and susceptibility to inflammation. J Immunol 2008;180(4):2588–2599.
39. Walker F, Zhang H-H, Odorizzi A, et al. LGR5 is a negative regulator of tumourigenicity, antagonizes Wnt signalling and regulates cell adhesion in colorectal cancer cell lines. PLoS One 2011;6(7):e22733.
40. Vicente-Dueñas C, Gutiérrez de Diego J, Rodrígues FD, et al. The role of cellular plasticity in cancer development. Curr Med Chem 2009;16(28):3676–3685.
41. Wei L, Singh R, Ro S, et al. Gut microbiota dysbiosis in functional gastrointestinal disorders: Underpinning the symptoms and pathophysiology. JGH Open 2021; 5(9):976–987.
42. Waddell A, Ahrens R, Tsai Y-T, et al. Intestinal CCL11 and eosinophilic inflammation is regulated by myeloid cell-specific RelA/p65 in mice. J Immunol 2013; 190(9):4773–4785.
43. de Lau W, Kujala P, Schneeberger K, et al. Peyer's patch M cells derived from Lgr5(+) stem cells require SpiB and are induced by RankL in cultured "miniguts". Mol Cell Biol 2012;32(18):3639–3647.
44. Gaedcke J, Grade Marian, Jung K, et al. Mutated KRAS results in overexpression of DUSP4, a MAP-kinase phosphatase, and SMYD3, a histone methyltransferase, in rectal carcinomas. Genes Chromosomes Cancer 2010;49(11):1024–1034.
45. Skrzypczak M, Goryca K, Rubel T, et al. Modeling oncogenic signaling in colon tumors by multidirectional analyses of microarray data directed for maximization of analytical reliability. PLoS One 2010;5(10).
46. Hong Y, Downey T, Eu KW, et al. A 'metastasis-prone' signature for early-stage mismatch-repair proficient sporadic colorectal cancer patients and its implications for possible therapeutics. Clin Exp Metastasis 2010; 27(2):83–90.
47. Cancer Genome Atlas Newtork. Comprehensive molecular characterization of human colon and rectal cancer. Nature 2012;487(7407):330–337.
48. Kaiser S, Park Y-K, Franklin JL, et al. Transcriptional recapitulation and subversion of embryonic colon development by mouse colon tumor models and human colon cancer. Genome Biol 2007;8(7):R131.
49. Graudens E, Boulanger V, Mollard C, et al. Deciphering cellular states of innate tumor drug responses. Genome Biol 2006;7(3):R19.
50. Ki DH, Jeung H-C, Park CH, et al. Whole genome analysis for liver metastasis gene signatures in colorectal cancer. Int J Cancer 2007;121(9):2005–2012.
51. Gaspar C, Cardoso J, Franken P, et al. Cross-species comparison of human and mouse intestinal polyps reveals conserved mechanisms in adenomatous polyposis coli (APC)-driven tumorigenesis. Am J Pathol 2008; 172(5):1363–1380.
52. Notterman DA, Alon U, Sierk AJ, et al. Transcriptional gene expression profiles of colorectal adenoma, adenocarcinoma, and normal tissue examined by oligonucleotide arrays. Cancer Res 2001;61(7): 3124–3130.
53. Sabates-Bellver J, Van der Flier LG, de Palo M, et al. Transcriptome profile of human colorectal adenomas. Mol Cancer Res 2007;5(12):1263–1275.
54. Cyphert JM, Allen IC, Church RJ, et al. Allergic inflammation induces a persistent mechanistic switch in thromboxane-mediated airway constriction in the mouse. Am J Physiol Lung Cell Mol Physiol 2012; 302(1):L140–L151.
55. Williams TM, Leeth RA, Rothschild DE, et al. The NLRP1 inflammasome attenuates colitis and colitis-associated tumorigenesis. J Immunol 2015;194(7):3369–3380.
56. Allen IC, Lich JD, Arthur JC, et al. Characterization of NLRP12 during the development of allergic airway disease in mice. PLoS One 2012;7(1):e30612.
57. Lee SM, Kim N, Son HJ, et al. The Effect of Sex on the Azoxymethane/Dextran Sulfate Sodium-treated Mice Model of Colon Cancer. J Cancer Prev 2016;21(4):271–278.
58. Williams TM, Leeth RA, Rithschild DE, et al. Caspase-11 attenuates gastrointestinal inflammation and experimental colitis pathogenesis. Am J Physiol Gastrointest Liver Physiol 2015;308(2):G139–G150.
59. Meira LB, Bugni JM, Green SL, et al. DNA damage induced by chronic inflammation contributes to colon carcinogenesis in mice. J Clin Invest 2008; 118(7):2516–2525.
60. Rothschild DE, Srinivasan T, Aponte-Santiago LA, et al. The Ex Vivo Culture and Pattern Recognition Receptor Stimulation of Mouse Intestinal Organoids. J Vis Exp 2016:111.
61. Schmittgen TD, Livak KJ. Analyzing real-time PCR data by the comparative C(T) method. Nat Protoc 2008; 3(6):1101–1108.

Received June 23, 2023. Accepted May 7, 2024.

Correspondence
Address correspondence to: Irving Coy Allen, PhD, 295 Duckpond Drive, Blacksburg, Virginia 24061. e-mail: icallen@vt.edu.

Acknowledgments
The authors thank Dr Sheryl Coutermarsh-Ott, Bettina Heid, Hannah Ivester, Khan Mohammad Imran, Juselyn Tupik, Margaret Nagai-Singer, Benjamin Tintera, and Kacie Hoyt for their technical support. They thank the College of Veterinary Medicine Teaching and Research Animal Care Support Service, Dr Al Baldwin for providing the *RelA*$^{fl/fl}$ mice, and Amgen and Dr Vanessa Redecke for providing the *Nik*$^{-/-}$ mice. They also thank Drs Jean Peccoud and Neil Adames for assistance conceptualizing the *Nik*$^{fl/fl}$ targeting constructs. They appreciate the assistance of Drs Dario Sorrentino and Vu Nguyen with human clinical specimen acquisition.

CRediT Authorship Contributions
Holly Ann Morrison (Conceptualization: Equal; Data curation: Equal; Formal analysis: Equal; Investigation: Equal; Methodology: Equal; Visualization: Equal; Writing – original draft: Equal; Writing – review & editing: Equal)
Kristin Eden (Data curation: Equal; Formal analysis: Equal; Investigation: Equal; Methodology: Equal; Visualization: Equal; Writing – original draft: Equal; Writing – review & editing: Equal)
Brie Trusiano, DVM, DACVP (clinical) (Writing – review & editing: Equal)
Daniel E. Rothschild (Data curation: Supporting; Methodology: Supporting; Writing – review & editing: Supporting)
Yufeng Qin (Data curation: Supporting; Formal analysis: Supporting; Methodology: Supporting; Software: Supporting)
Paul A. Wade (Data curation: Supporting; Formal analysis: Supporting; Methodology: Supporting; Software: Supporting; Writing – review & editing: Supporting)
Audrey J. Rowe (Data curation: Supporting; Writing – review & editing: Supporting)
Christina Mounzer (Data curation: Supporting; Writing – review & editing: Supporting)

Morgan C. Stephens (Data curation: Supporting; Writing – review & editing: Supporting)

Katherine M. Hanson (Data curation: Supporting; Methodology: Supporting; Resources: Supporting)

Stephan L Brown (Data curation: Supporting; Methodology: Supporting; Resources: Supporting)

Eda K. Holl (Data curation: Supporting; Methodology: Supporting; Resources: Supporting; Collected and provided human specimens: Lead)

Irving C. Allen (Data curation: Lead; Formal analysis: Lead; Funding acquisition: Lead; Investigation: Lead; Methodology: Lead; Project administration: Lead; Resources: Lead; Software: Lead; Supervision: Lead; Validation: Lead; Visualization: Lead; Writing – original draft: Equal; Writing – review & editing: Equal)

Conflicts of interest

The authors disclose no conflicts.

Funding

Supported by the NIH (R03DK105975; NCATS iTHRIVE UL1TR003015), The Virginia-Maryland College of Veterinary Medicine, The Via College of Osteopathic Medicine, and The Virginia Tech Carilion School of Medicine. The content is solely the responsibility of the authors and does not necessarily represent the official views of the NIH or any other funding body.

Data Availability

Data have been deposited in the GEO repository (Accession Number: GSE227993). https://www.ncbi.nlm.nih.gov/geo/query/acc.cgi?acc=GSE227993